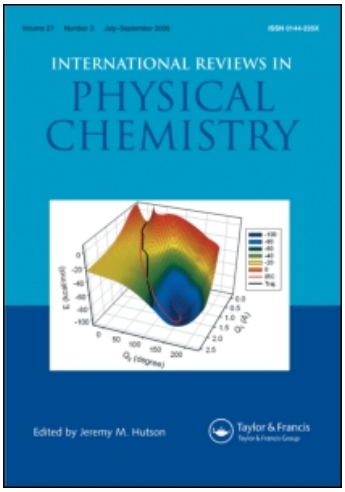

International Reviews in Physical Chemistry
Publication details, including instructions for authors and subscription information:
http://www.informaworld.com/smpp/title~content=t713724383

Role of angular momentum in statistical unimolecular rate theory

Eric E. Aubanel[a]; David M. Wardlaw[a]; Ling Zhu[b]; William L. Hase[b]
[a] Department of Chemistry, Queen's University, Kingston, Ontario, Canada [b] Department of Chemistry, Wayne State University, Detroit, MI, USA

To cite this Article Aubanel, Eric E. , Wardlaw, David M. , Zhu, Ling and Hase, William L.(1991) 'Role of angular momentum in statistical unimolecular rate theory', International Reviews in Physical Chemistry, 10: 3, 249 — 286
To link to this Article: DOI: 10.1080/01442359109353259
URL: http://dx.doi.org/10.1080/01442359109353259

INTERNATIONAL REVIEWS IN PHYSICAL CHEMISTRY, 1991, VOL. 10, NO. 3, 249–286

Role of angular momentum in statistical unimolecular rate theory†

by ERIC E. AUBANEL and DAVID M. WARDLAW
Department of Chemistry, Queen's University,
Kingston, Ontario K7L 3N6, Canada

LING ZHU and WILLIAM L. HASE
Department of Chemistry, Wayne State University,
Detroit, MI 48202, USA

A variety of topics is reviewed with an emphasis on assessment of models and discussion of their underlying physical assumptions, rather than on an overview of applications. Different treatments of angular momentum in the Rice–Ramsperger–Kassel–Marcus theory are surveyed and compared for tight and flexible transition states. The influence of angular momentum on thermal reaction rates is examined within the framework of variational transition state theory. The vibrational/rotational adiabatic theory of unimolecular decomposition is discussed. Various models for product energy distributions are summarized. The nature of non-thermal distributions of reactant angular momentum, arising from particular experimental techniques, is examined. A brief discussion of theoretical studies of vibrational/rotational coupling in the reactant and at the transition state is provided. The review attempts to unify advances in the fields of neutral and ion unimolecular decomposition.

1. Introduction

One of the goals of unimolecular rate theory has been the development of accurate theoretical models for calculating properties of unimolecular reactions. The monoenergetic unimolecular rate constant $k(E)$ and the partitioning of energy between unimolecular reaction products are two properties which have been treated by theoretical models. An important feature of any theoretical model are the assumptions regarding the relative importance of dynamical versus statistical effects. Rice–Ramsperger–Kassel–Marcus (RRKM) theory assumes (Robinson and Holbrook 1972, Forst 1973, Hase 1976a, b) that only statistical sums and densities of states need be considered in calculating $k(E)$. Overall, RRKM theory has been quite successful in reproducing experimental unimolecular rate constants. Phase space theory (Pechukas and Light 1965, Pechukas, Light and Rankin 1966), a model for calculating product energy partitioning, also assumes that only statistical effects are important, but it has been much less successful than RRKM theory (Marcus 1975, Worry and Marcus 1977).

Improvements in statistical models of unimolecular decomposition were made by researchers treating either neutral or ion decomposition. One of the shortcomings of unimolecular rate theory has been the lack of communication between those studying these two types of reactants. In many respects, the unimolecular kinetics of neutrals and ions are nearly independent research fields. As a result, researchers in one field have often failed to recognize and use advances made in the other. This has certainly not

†Dedicated to Walter J. Chesnavich, *in memoriam*.

0144-235X/91 $3·00

been beneficial in the development of an accurate statistical theory for unimolecular decomposition. In this review, one goal is to give a presentation which unifies the advances made in the fields of neutral and ion unimolecular decomposition.

The remainder of this review is organized as follows. Different treatments of angular momentum in RRKM theory are surveyed and compared in sections 2 and 3. Application of RRKM theory to thermal unimolecular reactions is reviewed in section 4. The vibration/rotational adiabatic theory of unimolecular decomposition is discussed in section 5. Section 6 surveys the different types of reactant angular momentum distributions which arise from non-thermal experimental conditions. Models for product energy partitioning in unimolecular dissociation are compared in section 7. A brief survey of experimental and theoretical studies of vibrational/rotational coupling is given in the concluding section.

2. Survey of the treatment of angular momentum in RRKM theory

In the initial development of statistical theoretical models more emphasis was placed on accurately treating the total energy E than the total angular momentum J. This is illustrated by the original RRKM expression (Marcus and Rice 1951, Marcus 1952) for $k(E)$, i.e.

$$k(E)=\frac{Q^{\dagger}_{\mathrm{rot}}}{Q_{\mathrm{rot}}}\frac{G(E^{\dagger}_{v})}{hN(E^{\dagger}_{v}+E_0)}, \tag{1}$$

where $Q^{\dagger}_{\mathrm{rot}}/Q_{\mathrm{rot}}$ is the ratio of transition state and reactant partition functions for the 'adiabatic' external rotations, $E^{\dagger}_{v}$ is the vibrational energy of the transition state, E_0 is the unimolecular threshold, $G(E^{\dagger}_{v})$ is the sum of 'active' internal states for the transition state, and $N(E^{\dagger}_{v}+E_0)$ is the density of states for the reactant 'active' modes. Following earlier work by Rice and Gershinowitz (1934), the ratio of external rotational partition functions is assumed to account for the effect of rotational angular momentum. It was recognized that equation (1) is incomplete (Weider and Marcus 1962). When equation (1) is incorporated into Lindenmann–Hinshelwood theory, the correct high-pressure thermal rate expression results, but the expression for the low-pressure limit is incorrect. In addition, equation (1) does not provide an interpretation of unimolecular rate constants as a function of total angular momentum J (Bunker and Pattengill 1968).

Improvements to equation (1), which explicitly treat angular momentum, have been principally directed to two different types of unimolecular transition states. For 'vibrator' transition states the transition state internal degrees of freedom are treated as vibrational modes and torsions with no barriers to internal rotation. In the second type of transition state, the dissociating fragments are held together by weak forces and rocking/bending degrees of freedom are treated as rotations. This latter type was initially called an 'orbiting' transition state (Chesnavich and Bowers 1979). However, a better name, which also includes the orbiting concept, is 'flexible' transition state (Aubanel and Wardlaw 1989).

The importance of angular momentum was recognized in developing variational RRKM theory (Bunker and Pattengill 1968, Hase 1983). Here the transition state is located at the minimum in the sum of states along the reaction path. For unimolecular reactions with well-defined potential energy barriers, the variational transition state is normally at the barrier maximum. Reactions with flexible transition states or vibrator transition states with low vibrational frequencies usually have poorly defined barriers, if any at all, and the variational criterion is of utmost importance in placing the transition state.

In the following, treatments of angular momentum for unimolecular reactions with vibrator and flexible transition states are reviewed. The variational criterion is not explicitly considered. However, some of the expressions presented for the sum of states may be used to determine variational transition state structures.

2.1. *Vibrator transition states*

Energy was assumed to be separable between vibration and rotation in initial treatments of angular momentum for unimolecular decomposition with vibrator transition states. The energy in the active modes (usually all of the vibrations and internal rotations) of the energized molecule is denoted by E_v, while the energy for the adiabatic external rotations is E_r. The energy for the active modes of the transition state is

$$E^\dagger = E_v + E_r - E_r^\dagger - E_0. \tag{2}$$

These energies are depicted in figure 1. With this treatment for angular momentum, the unimolecular rate constant becomes a function of both E_v and E_r and is (Marcus 1965)

$$k(E_v, E_r) = \frac{1}{h}\frac{G(E_v + E_r - E_r^\dagger - E_0)}{N(E_v)}. \tag{3}$$

If the pseudo-diatomic approximation is made for the external rotations (Marcus 1965), E_r becomes

$$E_r = \frac{\hbar^2}{2I} J(J+1), \tag{4}$$

where I is the principal moment of inertia for the reactant approximated as a diatomic. An illustration of this approximation is $I = \mu r^2$ for C_2H_6, where r is the separation between the centres of mass of the CH_3 moieties and μ is their reduced mass. (In this article the symbol J will be used for both the magnitude of the total angular momentum and the principal rotational quantum number. The authors recognize that this may lead to some confusion. However, the use of J for these two quantities is so pervasive that any other approach would be even more confusing.) Since total angular momentum is conserved during the unimolecular decomposition, the rotational energy

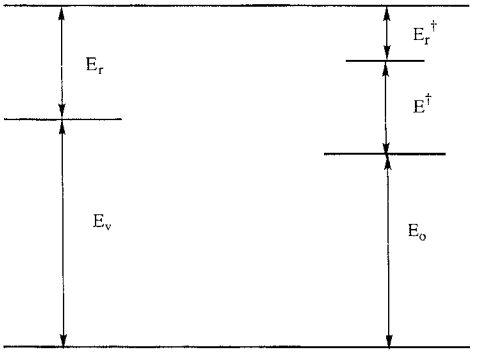

Figure 1. RRKM theory energy level diagram for a vibrator transition state.

of the transition state is given by $E_r^\dagger = E_r(I/I^\dagger)$. The active internal energy for the transition state is then

$$E^\dagger = E_v + E_r(1 - I/I^\dagger) - E_0. \tag{5}$$

Equations (3)–(5) constitute the treatment of angular momentum given in many textbooks (Robinson and Holbrook 1972, Steinfeld *et al.* 1989).

For a thermal distribution of reactant rotational energies, the average unimolecular rate constant was written (Bunker and Pattengill 1968) as

$$k(E_v, T_{\text{rot}}) = \int k(E_v, E_r)P(E_r)\,\mathrm{d}E_r. \tag{6}$$

Equations (3), (5) and (6) were used to interpret classical trajectory simulations of the dissociation of triatomics rotating in a plane (Bunker and Pattengill 1968). Three-dimensional external rotation was treated (Bunker 1972) by assuming the rotational energy can be represented by the classical expression

$$E_r = \sum_{i=1}^{3} J_i^2/2I_i.$$

Equations (2) and (3) are then used to calculate $k(E_v, E_r)$. If the principal rotation axes are the same for the molecule and transition state (Hase, Buckowski and Swamy 1983),

$$E^\dagger = E_v + \sum_{i=1}^{3} E_{ri}\left(1 - \frac{I_i}{I_i^\dagger}\right) - E_0. \tag{7}$$

In employing equations (2) and (3) to calculate thermal unimolecular rate constants versus pressure and temperature, it was proposed (Marcus 1965) that average values be used for E_r and $E_r^\dagger$ instead of integrating over E_r as is done in equation (6). At the high-pressure limit $\langle E_r^\dagger \rangle$ was found to equal lRT/2, where $l=2$ for the pseudo-diatomic approximation, equation (4). This relationship is approximately correct as the pressure is lowered. The average unimolecular rate constant is given by

$$k(E_v, T_{\text{rot}}) = \frac{1}{h}\frac{G(E_v + l\text{RT}/2[I^\dagger/I - 1] - E_0)}{N(E_v)}, \tag{8}$$

where $I^\dagger/I$ is the ratio of the moments of inertia for the degrees of freedom concerned. [For asymmetric tops, I and $I^\dagger$ are determined from the appropriate root of the product of the principal moments of inertia, e.g. $I = (\prod_{i=1}^{n} I_i)^{1/n}$.] Equation (8) has been widely used in calculating unimolecular fall-off curves (Waage and Rabinovitch 1970). It is incorrect to use equation (8) for non-thermal unimolecular systems (Hase 1976). For large non-thermal values of E_v, $k(E_v, E_r)$ becomes independent of E_r and the average rotational energy of the reacting molecules $\langle E_r \rangle$ becomes equal to the average of the thermal rotational energy distribution lRT/2, instead of $(I^\dagger/I)l$RT/2 as given by equation (8). Only for concomitant thermal vibrational and rotational distributions is it correct to use the latter expression for $\langle E_r \rangle$. For most non-thermal experiments it is probably better to explicitly integrate over E_r as is done in equation (6) than assume an average value for either E_r or $E_r^\dagger$.

Equation (7) and the use of $l=3$ in equation (8) notwithstanding, the principal focus in the above discussion has been on a pseudo-diatomic model with two external rotational degrees of freedom. The third rotational degree of freedom present for

nonlinear polyatomic molecules is simply neglected. It is instructive to criticize this pseudo-diatomic model by considering a symmetric top, whose rotational energy levels depend on the quantum numbers J and K according to

$$E_r(J,K)=\frac{J(J+1)\hbar^2}{2I_a}+\frac{K^2\hbar^2}{2}\left(\frac{1}{I_c}-\frac{1}{I_a}\right), \tag{9}$$

where $I_a=I_b\neq I_c$. In the previous pseudo-diatomic model, the J-dependent term is assumed to be adiabatic. If the K-dependent term is also assumed to be adiabatic, the unimolecular rate constant for a symmetric top is written as

$$k(E,J,K)=\frac{1}{h}\frac{G[E-E_0-E_r^{\dagger}(J,K)]}{N[E-E_r(J,K)]}. \tag{10}$$

For $K=0$, equation (10) gives the same rate constant as does the pseudo-diatomic model. To determine $k(E,J)$ from equation (10), a microcanonical average over K is required to give

$$k(E,J)=\sum_{K=-J}^{J}N(E,J,K)k(E,J,K)/h\sum_{K=-J}^{J}N(E,J,K), \tag{11a}$$

$$k(E,J,K)=\sum_{K=-J}^{J}G[E-E_0-E_r^{\dagger}(J,K)]/h\sum_{K=-J}^{J}N(E,J,K), \tag{11b}$$

where $N(E,J,K)=N[E-E_r(J,K)]$.

By assuming each K has an equal probability, equation (11) becomes

$$k(E,J)=\sum_{K=-J}^{J}k(E,J,K)/(2J+1). \tag{12}$$

In equations (11) and (12) the rate constant is written as a function of E and J instead of E_v and E_r, as in equations (2)–(8). This is because, by averaging over K, the total energy at a constant J cannot be written as a sum of E_v and E_r. Equations (10)–(12) represent general adiabatic treatments of angular momentum for symmetric tops. They have not been widely used to calculate unimolecular rate constants. However, if J is small and/or the unimolecular rate constant is rather insensitive to K, the pseudo-diatomic model, equations (2)–(5), is expected to give a rate constant similar to that for equation (12). Rate constants determined from these two approaches are compared in section 3.

In most applications of RRKM theory, the K quantum number is assumed to be active. Two different approaches have been advanced to accomplish this (Zhu and Hase 1990). One approach, initially presented in studies of C_2H_5 decomposition (Schneider and Rabinovitch 1962, Current and Rabinovitch 1963), is to maintain the use of equation (3) for $k(E_v,E_r)$ and to make the energy of the K-dependent term

$$E_r(K)=\frac{K^2\hbar^2}{2}\left(\frac{1}{I_c}-\frac{1}{I_a}\right) \tag{13}$$

active (Forst 1973). The argument made is that, for symmetric (or nearly symmetric) top reactive systems, external rotation about the symmetry axis should strongly couple with the internal degrees of freedom. Thus, this one external rotation should be treated as an active mode. The sum of states for the transition state and density of states for the

molecule are then written as convolutions between the densities and sums of states for the internal degrees of freedom and the active external rotation:

$$G(E^\dagger)=\int_0^{E^\dagger} G_{\text{vib}}(E)N_{\text{rot}}(E^\dagger-E)\,\mathrm{d}E, \tag{14a}$$

$$N(E_v)=\int_0^{E_v} N_{\text{vib}}(E)N_{\text{rot}}(E_v-E)\,\mathrm{d}E, \tag{14b}$$

where E_v is the active energy for the energized reactant and $E^\dagger$ given by equation (2), is the active energy of the transition state. The adiabatic rotational energies E_r and $E_r^\dagger$ are given by equation (4), and the total energy is given by $E=E_v+E_r$. This model is the same as the above pseudo-diatomic model, except the third rotational degree of freedom is no longer neglected, but made active. A shortcoming of this model is that the proper restrictions are not placed on K, i.e. $-J\leqslant K\leqslant J$, as a result of the free exchange of energy with the K-dependent term.

In the second approach (Quack and Troe 1974, Miller 1979, Troe 1983) for treating the K-dependent term as an active degree of freedom, the proper limits are placed on the K quantum number. The density of states for the energized reactant and the sum of states for the transition state are found for total energy E and angular momentum J by summing over contributions from all possible values of K, i.e.

$$G(E^\dagger,J)=\sum_{K=-J}^{J} G[E-E_0-E_r^\dagger(J,K)] \tag{15a}$$

$$N(E,J)=\sum_{K=-J}^{J} N[E-E_r(J,K)], \tag{15b}$$

where $E_r(J,K)$ is given by equation (9) and a similar expression is used for $E_r^\dagger(J,K)$. For 'almost' symmetric tops, where $I_a\approx I_b$, one can use the approximation (Townes and Schalow 1955)

$$E_r(J,K)=(I_a^{-1}+I_b^{-1})[J(J+1)-K^2]\hbar^2/4+K^2\hbar^2/2I_c \tag{16}$$

for the rotational energy. The unimolecular rate constant is written as

$$k(E,J)=\frac{1}{h}\frac{G(E^\dagger,J)}{N(E,J)} \tag{17}$$

and is seen to be identical in form to $k(E,J)$ for an adiabatic treatment of the K quantum number [i.e. equation (11)].

If the variational criterion is not used so that the transition state is fixed along the reaction path, $k(E,J)$ for the K-adiabatic model, equation (11), is analytically identical to $k(E,J)$ for the second K-active model. However, if the variational criterion is applied, this will not be the case. When applying the variational criterion to the K-adiabatic model, the $G[E-E_0-E_r^\dagger(J,K)]$ in equation (10) is chosen to be a minimum along the reaction path for fixed E, J and K. Thus $k(E,J)$ in equation (11) will be determined by a summation of these minimum sums of state. For the second K-active model, the variational criterion involves finding the minimum in $G(E^\dagger,J)$ [equation (15 a)], which is a summation over contributions from all possible values of K. Therefore, for the K-adiabatic model each $G(E^\dagger,J,K)$ sum is minimized, but for the K-active model the total sum $G(E^\dagger,J)$ is minimized. The K-adiabatic model will give a variational $k(E,J)$ which is less than or equal to that of the second K-active model.

At first glance, one might suspect that the second model, equation (15), is superior for treating the K quantum number as an active degree of freedom. However, this is not necessarily so, since a coriolis vibration–rotation interaction can be accounted for, in approximate fashion, but the first model, equation (14), but not by the second. For many molecules, the moment of inertia for the symmetry axis is strongly dependent on the vibrational energy. An example is C_2H_6, for which rather modest changes in the positions of the H-atoms can easily raise or lower the symmetry axis moment of inertia by a factor of two. Such an effect will lead to extensive energy sharing between vibration and the K-dependent part of the rotation. This energy sharing is treated in restrictive fashion by the second model but in unrestrictive fashion by the first. Quantitative comparisons between these two models are made in section 3.

For some analyses (e.g. interpreting classical trajectory simulation), one may wish to use the classical mechanical analogues of the above models in treating angular momentum. The classical rotational energy can be used directly when calculating $k(E_v, E_r)$, equation (3), and averaging over E_r, equation (6), for the 2-dimensional external rotation model. These equations are also applicable to 1-dimensional planar rotation, and an analytic expression has been obtained (Bunker and Pattengill 1968) for $k(E_v, T_{rot})$, equation (5), with a 1-dimensional thermal rotational energy distribution. Rotational energy may also be treated classically in the two 3-dimensional external rotation models which make the symmetric rotation axis an active degree of freedom. In the model which assumes that energy flows freely between vibrational modes and the active external rotation, equation (14), the classical expression (Forst 1973)

$$N_{rot}(E)=\frac{1}{\hbar}(8\pi^2 I/E)^{1/2} \tag{18}$$

is used for the rotational density of states. The classical analogue for the 3-dimensional model with proper constraints on the quantum number K, equation (15), is to make K a continuous variable so that

$$G(E^\dagger, J)=\int_{-J}^{J} G[E-E_0-E_r^\dagger(J,K)]\,\mathrm{d}K, \tag{19a}$$

$$N(E,J)=\int_{-J}^{J} N[E-E_r(J,K)]\,\mathrm{d}K. \tag{19b}$$

2.2. *Flexible transition states*

In unimolecular bond ruptures and ion-molecule dissociations such as $C_2H_6 \rightarrow 2CH_3$ and $Cl^-(CH_3Cl) \rightarrow Cl^- + CH_3Cl$, the long-range intermolecular forces between the dissociation fragments are very weak and highly flexible. A model often assumed (Wardlaw and Marcus 1988) for such reactions is that the long-range Hamiltonian is separable and can be written as

$$H=H_{v1}+H_{v2}+T_{r1}+T_{r2}+\frac{l^2}{2\mu R^2}+E_t+V \tag{20}$$

where the subscripts v and r signify vibrational and rotational motion for the two fragments, T is rotational kinetic energy, l is the orbital angular momentum, μ is the reduced mass for the two fragments, R is the fragment–fragment centre-of-mass separation, E_t is the relative translational energy projected on the centre-of-mass

separation and V, which depends on R and the relative orientation of the two fragments, is the intermolecular potential. The unimolecular system's total angular momentum J is a vector sum of the rotational angular momenta j_1 and j_2 for the two fragments and the orbital angular momentum l, i.e.

$$\boldsymbol{J}=\boldsymbol{j}_1+\boldsymbol{j}_2+\boldsymbol{l}. \tag{21}$$

It is often convenient to couple j_1 and j_2 to obtain the total rotational angular momentum

$$\boldsymbol{J}_r=\boldsymbol{j}_1+\boldsymbol{j}_2. \tag{22}$$

Most unimolecular bond ruptures and ion-molecule dissociations have no potential barrier (or only a poorly defined barrier) in the long-range intermolecular potential. For such cases, the variational version of RRKM theory (Hase 1983), which locates the transition state at the minimum in the sum of states along the reaction path, should be used. The energy level spacings for the rotational and orbital motions of the two fragments are quite small and it is often an excellent approximation to treat these motions classically (Wardlaw and Marcus 1988, Klippenstein and Marcus 1987, Hase and Wardlaw 1989). In contrast, the vibrational frequencies for the two fragments are usually sufficiently high that the vibrational energy $H_v=H_{v1}+H_{v2}$ must be treated quantum mechanically. Thus, the sum of states along the reaction path is written as the convolution

$$G(E^\dagger, J)=\int_0^{E^\dagger} G_v(E^\dagger-E_r)N_r(E_r)\,\mathrm{d}E_r, \tag{23}$$

where $G_v(E^\dagger-E_r)$ is the quantum mechanical sum of states for the intramolecular vibrational motions of the two fragments, $N_r(E_r)$ is the classical density of states for the fragments of intermolecular rotational/orbital motions, $E^\dagger=E-V(R)$, and $V(R)$ is assumed to be the reaction path potential. (The authors realize that some confusion may arise from using the subscript r to represent the fragments rotational/orbital motions, as well as the reactant rotation, as in the previous section. However, in the original literature r is used for each of these rotations and it was felt additional confusion would arise by changing either symbol.) In solving equation (23), two boundary conditions, due to conservation of total angular momentum, equations (21) and (22), arise, and are given by

$$|l-J_r|\leqslant J\leqslant l+J_r, \tag{24a}$$

$$|j_1-j_2|\leqslant J_r\leqslant j_1+j_2. \tag{24b}$$

In the first treatments of unimolecular dissociations with flexible transition states ion-molecule dissociations were considered and the variational criterion was not used. Instead, a statistical unimolecular rate constant was formulated in terms of the association cross section for the two fragments by invoking the principle of detailed balance for the decomposition and association steps (Klots 1971, 1972, 1976, Chesnavich and Bowers 1977a, 1979). To calculate the association cross section it is assumed that the long-range potential is isotropic and given by

$$V(R)=-\frac{C}{R^n}. \tag{25}$$

The cross-section is determined using the Langevin model by choosing l, with J constant, so that the maximum in the effective potential $[l^2/2\mu R^2+V(R)]$ is equal to the

initial relative translational energy. By assuming the long-range potential is isotropic, one has to only consider the angular momentum constraints, and not the relative orientations of the fragments, in calculating the associated cross-section. Since trajectories orbit if placed at the maximum in the effective potential, the above treatment has often been referred to as an orbiting transition state model.

To outline this orbiting transition state model, the unimolecular reactant will be identifed by a and the product fragments by b. The cross-section associated with formation of a collision complex with angular momentum J, from reactants with relative translational energy E_t and rotational energy E_r^b, from Langevin theory, is (Chesnavich and Bowers 1977a, 1979)

$$\sigma_J(E_r^b, E_t) = \frac{\pi\hbar^2}{2\mu E_t} N_r^b(E_t, E_r^b, J), \tag{26}$$

where $N_r^b(E_t, E_r^b, J)$ is the density of angular momentum states in b for the conditions discussed above. The sum of angular momentum states at a given $E_{tr} = E_t + E_r^b$ is related to the above density by

$$G_r^b(E_{tr}, J) = \int N_r^b(E_t, E_r, J)\, dE_t. \tag{27}$$

By employing the principle of detailed balance, the unimolecular rate constant for decomposition of the collision complex to product fragments with relative translational energy E_t can be determined from the above cross section, equation (26), and is given by

$$k(E, J, E_t) = \frac{\sigma \int_{E_r^\ddagger}^{E-E_0} N_v^b(E - E_0 - E_t - E_r^b) N_r^b(E_t, E_r^b, J)\, dE_r^b}{hN(E - E_r^a)}, \tag{28}$$

when σ is the reactant to product symmetry number ratio and the lower limit on the integral, $E_r^\ddagger$, occurs at the minimum value of E_r^b for which $N_r^b(E_t, E_r^b, J) > 0$ at the fixed value of E_t.

Integrating equation (28) over E_t yields $k(E, J)$, which is given by

$$k(E, J) = \frac{\sigma \int_{E_{tr}^\ddagger}^{E-E_0} N_v^b(E - E_0 - E_{tr}) G_r^b(E_{tr}, J)\, dE_{tr}}{hN(E - E_r^a)}. \tag{29}$$

Here, the lower limit on the integral, $E_{tr}^\ddagger$, occurs at the minimum value of E_{tr} for which the sum of angular momentum states $G_r^b(E_{tr}, J) > 0$. The term $G_r^b(E_{tr}, J)$ can be written as

$$G_r^b(E_{tr}, J) = \int\int \Gamma(E_r^*, J_r)\, dJ_r\, dl, \tag{30}$$

where the sum of states $\Gamma(E_r^*, J_r)$ arises from the integration of the fragment rotational density of states $N_r(E_r, J_r)$ over E_r within the range defined by the angular momentum coupling restrictions of the Langevin model. The energy E_r^* is also defined by the Langevin model and is given by

$$E_r^* = E_{tr} - \frac{l^{2n/(n-2)}}{\lambda}, \tag{31}$$

when λ is a collection of constants. For $n = 4$, $\lambda = 16\mu^2 c/\hbar^4$.

Analytic expressions for $\Gamma(E_r^*, J_r)$ have been derived (Chesnavich and Bowers 1977b, 1979) for different types of fragments with the assumption that the long-range intermolecular potential is isotropic. The specific fragment types considered are linear–atom, sphere–atom, linear–linear, sphere–linear and sphere–sphere. For the purpose of obtaining $\Gamma(E_r^*, J_r)$, symmetric and asymmetric top fragments can be accurately represented by a spherical top, by using the root-mean moment of inertia in the appropriate expression for $\Gamma(E_r^*, J_r)$. For each of the above fragment types, the integration over J_r is analytic in equation (30), but the integrations over E_{tr} and l in equations (29) and (30) must be performed numerically.

It is useful to emphasize and review some of the features of the above model. First, the approach used is non-variational, so that the minimum in the sum of states along the reaction path is not used to find the transition state structure. Instead, it is assumed that the long-range intermolecular potential is isotropic and the transition state is placed at the centrifugal barrier. The assumption that the long-range potential is isotropic is most likely only valid for ion-molecule reactions dominated by isotropic ion-induced dipole potentials. For radical–radical and other types of ion-molecule reactions (e.g. ion-dipole) there is considerable anisotropy in the long-range potential. Also, in general the variational criterion does not locate transition states at rotational barriers. Reactions with isotropic long-range intermolecular potentials may be exceptions to this rule, but such a possibility has not been systematically investigated.

Variational RRKM calculations have been performed for the Hamiltonian in equation (20) with anisotropic intermolecular potentials (Wardlaw and Marcus 1984, 1985, 1986, 1988, Klippenstein and Marcus 1987, 1988, 1989, Aubanel and Wardlaw 1989, 1990, Song and Chesnavich 1989, 1990). To find the minimum in the sum of states along the reaction path, the density of states for the intermolecular rotational/orbital motions, $N_r(E_r)$ in equation (23), is treated classically and, for non-linear fragments, is given by

$$N_r(E_r) = (2J+1)(2\pi)^{-6}\sigma^{-1} \int \dots \int \mathrm{d}j_1\, \mathrm{d}j_2\, \mathrm{d}l\, \mathrm{d}J_r\, \mathrm{d}k_1\, \mathrm{d}k_2\, \mathrm{d}\alpha\, \Delta(J, J_r, l)\, \Delta(J_r, j_1, j_2)\, \delta(H_{CI} - E), \tag{32}$$

where $\mathrm{d}\alpha$ is the volume element for the angle variables conjugate to the angular momentum variables in equation (32), and σ is a symmetry number. The integrations over the angular momenta are restricted both by energy conservation and the triangle inequalities, equations (21) and (22), each Δ being unity when the relevant inequality is fulfilled and zero otherwise. The quantity k_i is the projection of j_i on an axis fixed in fragment i; this axis is most conveniently chosen to be one of the principal axes. If the fragment is a symmetric top, then k_i is most naturally taken to be the projection of j_i on the symmetry axis, simplifying the evaluation of equation (32). Each k_i is restricted by the condition $|k_i| \leqslant j_i$ and by energy conservation. H_{CI} is the part of the Hamiltonian in equation (19) that refers to the intermolecular rotational/orbital motions and is given by

$$H_{CI} = T_{r_1} + T_{r_2} + \frac{l^2}{2\mu R^2} + V. \tag{33}$$

Equations (15*b*), (16), (23) and (32) are used to calculate $k(E, J)$. Since the potential V depends on the relative orientation of the two fragments, evaluation of equation (23) via equation (32) is necessarily numerical; Monte Carlo integration methods have been effectively used in this regard.

3. Comparison of methods for calculating $k(E, J, K)$ and $k(E, J)$ RRKM rate constants

3.1. *Vibrator transition states*

In this section different methods are compared (Zhu and Hase 1990) for treating angular momentum when calculating RRKM unimolecular rate constants for reactive systems with a well-defined potential energy barrier at which a vibrator transition state is placed. If K is a good quantum number, the unimolecular rate constant for a symmetric top depends on E, J and K and is given by equation (10). The term $I_c^{-1} - I_a^{-1}$ in equation (9) is positive and negative for prolate and oblate tops, respectively. Thus, $E_r(J, K)$ increases for a prolate top and decreases for an oblate top, as K is increased. As a result, increasing K lowers the active vibrational energy for a prolate top, but increases it for an oblate top. Thus, for a fixed E and J, one expects the variation of the rate constant to depend on whether the reactive system is a prolate or oblate top.

The reactions $C_2H_5 \rightarrow H + C_2H_4$ and $C_6H_6 - H \rightarrow H + C_6H_6$ are used here to represent prolate and oblate systems, respectively. Each is treated as an 'almost' symmetric top according to equation (16). The reactant and transition state parameters used for ethyl radical decomposition have been given previously (Hase and Schlegel 1982). The parameters for the C_6H_6–H radical system, are those for an assumed model and are listed in table 1. To determine unimolecular rate constants, the Beyer–Swinehart algorithm (Beyer and Swinehart 1973, Stein and Rabinovich 1973) is used to make a direct count of sums of states for the transition states. The Whitten–Rabinovitch semi-empirical expression (Robinson and Holbrook 1972) is used to calculate densities of states for the energized reactants. Tests were made and show that using the Whitten–Rabinovitch approximation, instead of making direct counts of the state densities, results in rate constants that are in error by less than 5%.

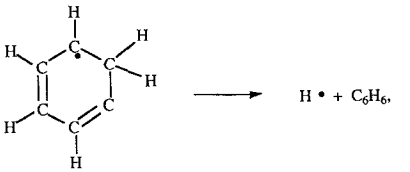

Table 1. Parameters for the C_6H_6–$H \rightarrow H + C_6H_6$ model system.

	Radical		Transition state	
Frequencies, cm^{-1}	3068	995	3068	995
	3063 (2)	992	3063 (2)	992
	3062	975 (2)	3062	975 (2)
	3047 (2)	849 (2)	3047 (2)	849 (2)
	1596 (2)	703	1596 (2)	703
	1486 (2)	673	1486 (2)	673
	1326	606 (2)	1326	606 (2)
	1310	410 (2)	1310	410 (2)
	1178 (2)	3058	1178 (2)	400
	1150	1079	1150	370
	1038 (2)	998	1038 (2)	
	1010		1010	
Moments of inertia, amu-$Å^2$	88·7, 88·7, 177·4		93·6, 93·6, 179·5	
Symmetry number	1		1	
E_0, kcal mol^{-1}	38·0			

3.1.1. *k(E, J, K) rate constants*

Rate constants were calculated for C_2H_5 dissociation versus K for values of the J quantum number equal to 5, 15 and 30, and for total energy E equal to 38·5, 40, 45 and 50 kcal mol^{-1}. For J equal to 5 the rate constant $k(E, J, K)$ is independent of K. Increasing J to 15 and 30 results in rate constants which depend on K, and the effects are illustrated in figures 2 and 3. As shown in figure 2, for $J = 15$ and $E = 38{\cdot}5$ kcal mol^{-1} there is an increase in $k(E, J, K)$ as K increases, until the rate constant becomes zero for $K > 9$. In contrast, for $J = 30$ and $E = 45$ and 50 kcal mol^{-1}, figure 3, $k(E, J, K)$ decreases as K is increased. For E of 38·5 and 40 kcal mol^{-1} and $J = 30$, the $k(E, J, K)$ are zero. The discontinuities in some of the $k(E, J, K)$ plots arise from discontinuities in the sum of states for the transition state at small values of $E^{\dagger} = E - E_0 - E_r^{\dagger}(J, K)$.

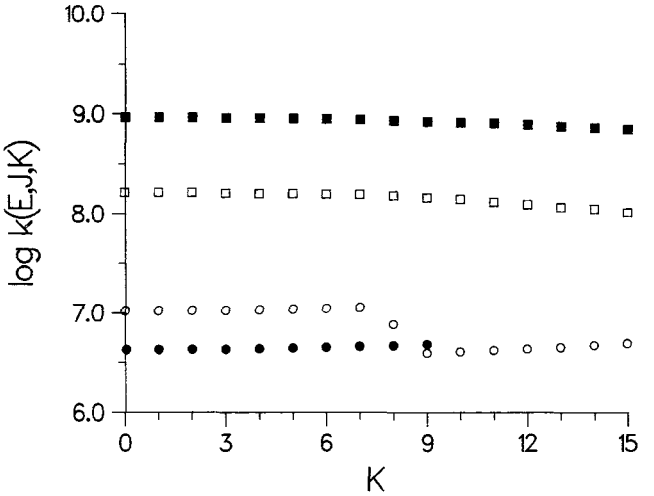

Figure 2. Plots of $k(E, J, K)$ for $C_2H_5 \rightarrow H + C_2H_4$ dissociation. $J = 15$ and E equals 38·5 (●), 40 (○), 45 (□), and 50 kcal mol^{-1} (■). For E of 38·5 kcal mol^{-1}, $k(E, J, K)$ is zero for $K > 9$.

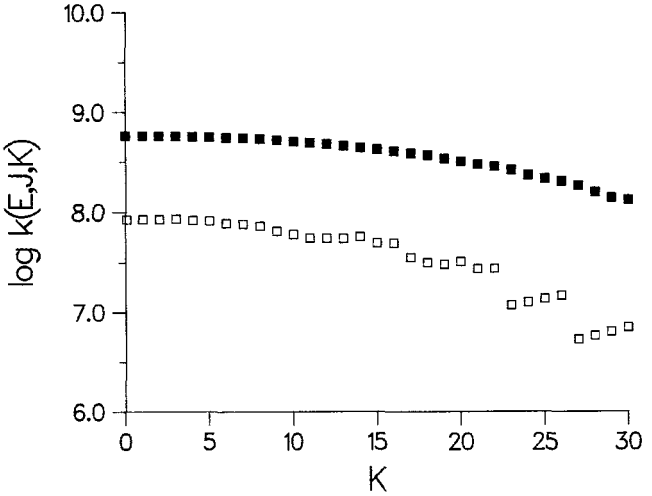

Figure 3. Same as figure 2, except $J = 30$. All the $k(E, J, K)$ are zero for E of 38·5 and 40 kcal mol^{-1}.

Values of $k(E, J, K)$ were calculated for C_6H_6–H decomposition as a function of K for $J=5$, 15 and 30 and $E=39$, 40, 45 and 50 kcal mol^{-1}. As found for C_2H_5 decomposition, for $J=5$ the rate constant $k(E, J, K)$ is insensitive to K. However, for $J=15$ and 30 the quantum number K does affect $k(E, J, K)$ as illustrated in figures 4 and 5. With $J=15$, the rate constant decreases with increase in K at the lowest energy of 39 kcal mol^{-1}, but increases with increase in K at the higher energies. Raising J to 30, results in $k(E, J, K)$ values which decrease with increase in K at 39 and 40 kcal mol^{-1}, but increase with increase in K at 45 and 50 kcal mol^{-1}.

The plots in figures 2–5 show that the K-dependence of the unimolecular rate constant is different for the C_2H_5 prolate top and C_6H_6–H oblate top systems. However, one should be careful before drawing any general conclusions from these

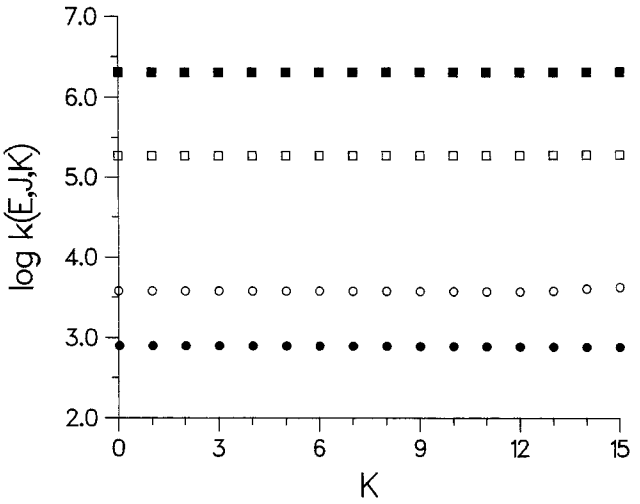

Figure 4. Plots of $k(E, J, K)$ for C_6H_6–H→H+C_6H_6 dissociation. $J=15$ and E equals 39 (●), 40 (○), 45 (□), and 50 kcal mol^{-1}.

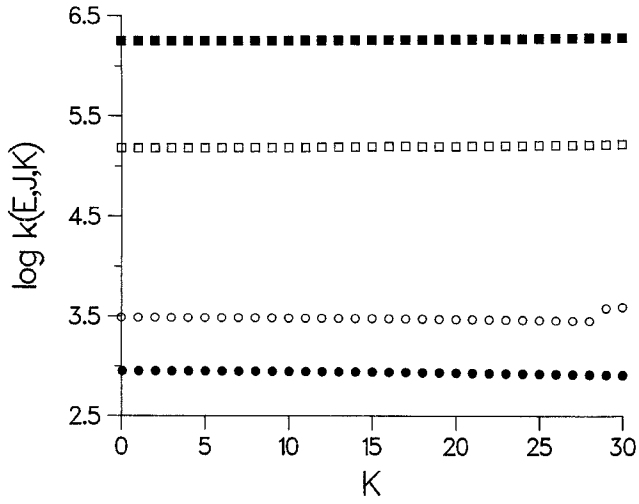

Figure 5. Same as figure 4, except $J=30$.

results. For example, the K-dependence of the rate constant is also affected by the relationship between the reactant and transition state moments of inertia. For the C_2H_5 system, $I_a \approx I_a^\dagger$ and $I_c < I_c^\dagger$. Thus, for C_2H_5 decomposition $E_r(J,K)$ will become increasingly larger than $E_r^\dagger(J,K)$ as K is increased. However, for the C_6H_6–H system $I_a \approx I_a^\dagger$ and $I_c \approx I_c^\dagger$, so that $E_r(J,K)$ and $E_r^\dagger(J,K)$ are approximately the same for all values of K. We expect that for most reactions an interpretation of the K-dependence of $k(E,J,K)$ will require an analysis of how both the sum of states and the density of states vary with K.

3.1.2. *$k(E,J)$ rate constants*

In section 2.1, adiabatic and active, and two- and three-dimensional angular momentum models are described for calculating $k(E,J)$. An additional approximate 3-dimensional adiabatic rotation model is considered here. However, instead of approximately averaging over K as is done in equation (12), an average rotational energy $\langle E_r(J)\rangle_K$ is subtracted from the total energy to give

$$k(E,J)=\frac{G(E-E_0-\langle E_r^\dagger(J,K)\rangle_K)}{hN(E-\langle E_r(J,K)\rangle_K)}. \tag{34}$$

The average rotational energy is written as

$$\langle E_r(J,K)\rangle_K = \sum_{K=-J}^{J} \frac{E_r(J,K)}{(2J+1)}, \tag{35a}$$

$$= \frac{J(J+1)\hbar^2}{2I_a} + \hbar^2(I_c^{-1}-I_a^{-1})\frac{\langle K^2\rangle}{2} \tag{35b}$$

$$\equiv \langle E_r(J)\rangle_K,$$

where

$$\langle K^2\rangle = \sum_{K=-J}^{J} \frac{K^2}{(2J+1)}. \tag{36}$$

For interpreting values of $k(E,J)$ it is useful to have an approximate rotational temperature T_r which corresponds to the value of J. A relationship between T_r and J is found from the thermal rotational energy, i.e.

$$\frac{3}{2}k_B T_r = \langle E_r(J)\rangle_K. \tag{37}$$

Using equations (35) and (36) yields

$$T_r = \frac{2J(J+1)\hbar^2(I_a^{-1}+I_c^{-1}/2)}{9k_B}. \tag{38}$$

The different models considered here for treating angular momentum when calculating $k(E,J)$ for vibrator transition states may be classified according to

2D/adiabatic	Equations (2)–(5)
3D/adiabatic	Equation (11)
3D/approx. adiabatic-I	Equation (12)
3D/approx. adiabatic-II	Equation (34)
3D/K, active-I	Equations (3), (14) and (18)
3D/K, active-II	Same as 3D/adiabatic

It should be noted, as discussed above, that the 3D/K, active-II model is only identical to the 3D/adiabatic model for fixed transition states.

To compare these models and to illustrate the effect of J on unimolecular rate constants, $k(E, J)$ values were determined for $C_2H_5 \rightarrow H + C_2H_4$, $C_6H_6{-}H \rightarrow C_6H_6 + H$, and $CH_3SiH_3 \rightarrow CH_4 + SiH_2$ dissociation, and are listed in tables 2–4. Sums and densities of state were evaluated as described above, and the reactants and transition state parameters used to calculate $k(E, J)$ values for C_2H_5 and $C_6H_6{-}H$ are those given above. *Ab initio* reactant and transition state parameters (Gordon and Truong 1987) are used to calculate $k(E, J)$ for $CH_3SiH_3 \rightarrow CH_4 + SiH_2$ dissociation.

The effects of J on the $k(E, J)$ values are mixed, and are amply illustrated by the calculations for C_2H_5 dissociation in table 2. At $E = 38{\cdot}5$ kcal mol^{-1} increasing J from 0 to 5 increases $k(E, J)$, which is also observed at $E = 40{\cdot}0$ kcal mol^{-1}. The effect observed by further increasing J to 15 at $E = 40{\cdot}0$ kcal mol^{-1} depends on the model. For some models $k(E, J)$ increases, while for others $k(E, J)$ decreases. At $E = 45$ kcal mol^{-1}, $k(E, J)$ for each model decreases as J is increased. The same result (not listed) was found for $E = 50$ kcal mol^{-1}. The results for $C_6H_6{-}H$ dissociation are the same as those for C_2H_5 dissociation, except at $E = 40$ kcal mol^{-1} where all the $k(E, J)$ values decrease with increase in J. Overall, the results for CH_3SiH_3 dissociation, table 4, mirror those for C_2H_5 and $C_6H_6{-}H$. At low levels of vibrational excitation and small values of J, the rate constant increases as J is increased. For larger values of E, $k(E, J)$ decreases with increases in J.

Table 2. Values of $k(E, J)$ predicted by different models for $C_2H_5 \rightarrow H + C_2H_4$†.

	Angular momentum quantum number J			
Model	0	5	15	30
		E = 38·5		
2D/adiabatic	$2{\cdot}56 \times 10^7$	$2{\cdot}59 \times 10^7$	0	0
3D/adiabatic	$2{\cdot}56 \times 10^7$	$2{\cdot}64 \times 10^7$	0	0
3D/approx. adiabatic-I	$2{\cdot}56 \times 10^7$	$2{\cdot}64 \times 10^7$	0	0
3D/approx. adiabatic-II	$2{\cdot}56 \times 10^7$	$2{\cdot}64 \times 10^7$	0	0
3D/K, active-I‡	$1{\cdot}25 \times 10^7$	$1{\cdot}26 \times 10^7$	0	0
		E = 40		
2D/adiabatic	$5{\cdot}72 \times 10^7$	$5{\cdot}79 \times 10^7$	$6{\cdot}30 \times 10^7$	0
3D/adiabatic	$5{\cdot}72 \times 10^7$	$5{\cdot}88 \times 10^7$	$4{\cdot}80 \times 10^7$	0
3D/approx. adiabatic-I	$5{\cdot}72 \times 10^7$	$5{\cdot}88 \times 10^7$	$4{\cdot}63 \times 10^7$	0
3D/approx. adiabatic-II	$5{\cdot}72 \times 10^7$	$5{\cdot}88 \times 10^7$	$2{\cdot}37 \times 10^7$	0
3D/K, active-I‡	$3{\cdot}11 \times 10^7$	$3{\cdot}13 \times 10^7$	$3{\cdot}32 \times 10^7$	0
		E = 45		
2D/adiabatic	$1{\cdot}27 \times 10^9$	$1{\cdot}23 \times 10^9$	$9{\cdot}88 \times 10^8$	$4{\cdot}98 \times 10^8$
3D/adiabatic	$1{\cdot}27 \times 10^9$	$1{\cdot}19 \times 10^9$	$8{\cdot}75 \times 10^8$	$3{\cdot}29 \times 10^8$
3D/approx. adiabatic-I	$1{\cdot}27 \times 10^9$	$1{\cdot}19 \times 10^9$	$8{\cdot}63 \times 10^8$	$2{\cdot}70 \times 10^8$
3D/approx. adiabatic-II	$1{\cdot}27 \times 10^9$	$1{\cdot}19 \times 10^9$	$8{\cdot}72 \times 10^8$	$2{\cdot}01 \times 10^8$
3D/K, active-I‡	$8{\cdot}16 \times 10^8$	$7{\cdot}88 \times 10^8$	$6{\cdot}27 \times 10^8$	$3{\cdot}03 \times 10^8$

† Rate constants and energy are in units of s^{-1} and kcal mol^{-1}, respectively. $J = 5$, 15 and 30 correspond to rotational temperatures of 47, 373 and 1447 K, respectively.

‡ The rate constants for the 3D/K, active-II model are the same as those for the 3D/adiabatic model.

Table 3. Values of $k(E, J)$ predicted by different models for C_6H_6–$H \rightarrow H + C_6H_6$†.

Model	Angular momentum quantum number J			
	0	17	50	97
		$E = 38{\cdot}5$ kcal mol		
2D/adiabatic	$8{\cdot}84 \times 10^2$	$9{\cdot}41 \times 10^2$	0	0
3D/adiabatic	$8{\cdot}84 \times 10^2$	$9{\cdot}31 \times 10^2$	0	0
3D/approx. adiabatic-I	$8{\cdot}84 \times 10^2$	$9{\cdot}31 \times 10^2$	0	0
3D/approx. adiabatic-II	$8{\cdot}84 \times 10^2$	$9{\cdot}31 \times 10^2$	0	0
3D/K, active-I‡	$4{\cdot}56 \times 10^2$	$4{\cdot}80 \times 10^2$	0	0
		$E = 40$ kcal mol		
2D/adiabatic	$4{\cdot}07 \times 10^3$	$3{\cdot}78 \times 10^3$	$8{\cdot}47 \times 10^2$	0
3D/adiabatic	$4{\cdot}07 \times 10^3$	$3{\cdot}74 \times 10^3$	$1{\cdot}28 \times 10^3$	0
3D/approx. adiabatic-I	$4{\cdot}07 \times 10^3$	$3{\cdot}75 \times 10^3$	$1{\cdot}22 \times 10^3$	0
3D/approx. adiabatic-II	$4{\cdot}07 \times 10^3$	$3{\cdot}74 \times 10^3$	$7{\cdot}78 \times 10^2$	0
3D/K, active-I‡	$2{\cdot}27 \times 10^3$	$2{\cdot}10 \times 10^3$	$4{\cdot}43 \times 10^2$	0
		$E = 45$ kcal mol		
2D/adiabatic	$2{\cdot}00 \times 10^5$	$1{\cdot}79 \times 10^5$	$9{\cdot}07 \times 10^4$	$4{\cdot}97 \times 10^3$
3D/adiabatic	$2{\cdot}00 \times 10^5$	$1{\cdot}83 \times 10^5$	$1{\cdot}06 \times 10^5$	$1{\cdot}64 \times 10^4$
3D/approx. adiabatic-I	$2{\cdot}00 \times 10^5$	$1{\cdot}83 \times 10^5$	$1{\cdot}05 \times 10^5$	$1{\cdot}37 \times 10^4$
3D/approx. adiabatic-II	$2{\cdot}00 \times 10^5$	$1{\cdot}83 \times 10^5$	$1{\cdot}07 \times 10^5$	$1{\cdot}18 \times 10^4$
3D/K, active-I‡	$1{\cdot}27 \times 10^5$	$1{\cdot}13 \times 10^5$	$5{\cdot}60 \times 10^4$	$2{\cdot}79 \times 10^3$

† Rate constants and energy are in units of s^{-1} and kcal mol^{-1}, respectively. $J = 17$, 50 and 97 correspond to rotational temperatures of 46, 387 and 1444 K, respectively.

‡ The rate constants for the 3D/K, active-II model are the same as those for the 3D/adiabatic model.

Table 4. Values of $k(E, J)$ predicted by different models for $CH_3SiH_3 \rightarrow CH_4 + SiH_2$†.

Model	Angular momentum quantum number J			
	0	5	15	30
		$E = 74$		
2D/adiabatic	$1{\cdot}04 \times 10^4$	$1{\cdot}04 \times 10^4$	$8{\cdot}63 \times 10^3$	$4{\cdot}82 \times 10^3$
3D/adiabatic	$1{\cdot}04 \times 10^4$	$1{\cdot}05 \times 10^4$	$6{\cdot}35 \times 10^3$	$1{\cdot}35 \times 10^3$
3D/approx. adiabatic-I	$1{\cdot}04 \times 10^4$	$1{\cdot}05 \times 10^4$	$6{\cdot}22 \times 10^3$	$1{\cdot}12 \times 10^3$
3D/approx. adiabatic-II	$1{\cdot}04 \times 10^4$	$1{\cdot}05 \times 10^4$	$6{\cdot}84 \times 10^3$	0
3D/K, active-I‡	$4{\cdot}05 \times 10^3$	$4{\cdot}06 \times 10^3$	$3{\cdot}32 \times 10^3$	$1{\cdot}77 \times 10^3$
		$E = 80$		
2D/adiabatic	$7{\cdot}42 \times 10^5$	$7{\cdot}34 \times 10^5$	$6{\cdot}75 \times 10^5$	$5{\cdot}17 \times 10^5$
3D/adiabatic	$7{\cdot}42 \times 10^5$	$7{\cdot}15 \times 10^5$	$5{\cdot}66 \times 10^5$	$3{\cdot}05 \times 10^5$
3D/approx. adiabatic-I	$7{\cdot}42 \times 10^5$	$7{\cdot}15 \times 10^5$	$5{\cdot}61 \times 10^5$	$2{\cdot}76 \times 10^5$
3D/approx. adiabatic-II	$7{\cdot}42 \times 10^5$	$7{\cdot}13 \times 10^5$	$5{\cdot}51 \times 10^5$	$2{\cdot}22 \times 10^5$
3D/K, active-I‡	$3{\cdot}61 \times 10^5$	$3{\cdot}57 \times 10^5$	$3{\cdot}27 \times 10^5$	$2{\cdot}47 \times 10^5$
		$E = 85$		
2D/adiabatic	$5{\cdot}59 \times 10^6$	$5{\cdot}55 \times 10^6$	$5{\cdot}26 \times 10^6$	$4{\cdot}39 \times 10^6$
3D/adiabatic	$5{\cdot}59 \times 10^6$	$5{\cdot}46 \times 10^6$	$4{\cdot}62 \times 10^6$	$2{\cdot}93 \times 10^6$
3D/approx. adiabatic-I	$5{\cdot}59 \times 10^6$	$5{\cdot}45 \times 10^6$	$4{\cdot}59 \times 10^6$	$2{\cdot}73 \times 10^6$
3D/approx. adiabatic-II	$5{\cdot}59 \times 10^6$	$5{\cdot}46 \times 10^6$	$4{\cdot}56 \times 10^6$	$2{\cdot}44 \times 10^6$
3D/K, active-I‡	$2{\cdot}99 \times 10^6$	$2{\cdot}96 \times 10^6$	$2{\cdot}80 \times 10^6$	$2{\cdot}32 \times 10^6$

† Rate constants and energy are in units of s^{-1} and kcal mol^{-1}, respectively. $J = 5$, 15 and 30 correspond to rotational temperatures of 25, 201 and 778 K, respectively.

‡ The rate constants for the 3D/K, active-II model are the same as those for the 3D/adiabatic model.

There are distinguishable relationships between the rate constants for the different models considered in table 2–4. The relationship between the rate constants for the 2D and 3D adiabatic models can be understood by considering the K-dependence of the rotational energy $E_r(J, K)$. Since $E_r(J, K)$ increases with K for a prolate top, the prolate top's average rotational energy at each J is larger for the 3D/adiabatic model than for the 2D/adiabatic model. Thus, for values of E and J where $k(E, J, K)$ decreases with increase in K, the $k(E, J)$ rate constants for the 3-D adiabatic models are expected to be smaller than those for the 2-D adiabatic model. This is the result observed for C_2H_5 and CH_3SiH_3 in tables 2 and 4, except for the smallest values of E and J. A similar line of reasoning for the C_6H_6–H oblate top system explains why the 2D/adiabatic rate constants are smaller than those calculated with the 3D/adiabatic model.

Of the two 3D/approx. adiabatic models, model I more accurately averages over K than does model II. Significant differences arise between these two models for large values of J, where model II gives rate constants substantially too small. A particularly interesting result is the extensive agreement found between the 3D/adiabatic model and 3D/approx. adiabatic-I model. For small values of J, the $k(E, J)$ for the two models are in exact agreement. As J is increased, the $k(E, J)$ for the correct adiabatic model become larger, but the largest difference observed here is only 20%. However, one expects the differences to increase as J is increased.

Of the two models which treat the K quantum number as an active degree of freedom, model I, which allows energy to flow freely between the K degree of freedom and the vibrations, has the smaller rate constant. As discussed in the previous section, if all anharmonic and vibrational rotation couplings are included in calculating the sum and density of states, the 3D/K, active-II model will give the correct microcanonical $k(E, J)$. However, these corrections are seldom made and are not made here. Thus, we are unable to judge which of the two K-active models gives the more accurate rate constant.

3.2. *Flexible transition states*

Sections 2.1 and 3.1 are concerned with vibrator transition states placed at well defined potential energy barriers. Such transition states are typically tight, meaning that the transition state structure does not deviate substantially from the reaction path geometry at the barrier maximum. The transition state structure thus has essentially constant moments of inertia in terms of which the overall (rigid rotor) rotational energy of the transition state is readily specified. If both the reactant and transition state can be modelled as symmetric tops with correlated moments of inertia, then it may be a good approximation to treat K as an adiabatic quantity. As the transition state loosens, its structure becomes less rigid and its moments of inertia are no longer constant. An example of this arises in the context of vibrator transition states: namely, the moment of inertia about the symmetry axis can be strongly dependent on the vibrational energy, e.g. C_2H_6. This presumably leads to extensive energy sharing between vibration and the K-dependent part of the overall rotation. For flexible transition states there are generally multidimensional hindered rotations of the two product fragments relative to each other; for truly loose transition states the fragments undergo free rotation. In such cases the transition state structure can only be defined in terms of the relative separation of the fragments since the moments of inertia for overall rotation of the transition state complex are not constant but depend on the fragments' relative orientation. The flexible transition state is not a single structure but is instead a set of numerous different structures each of which has different moments of inertia and different orientations of principal axes. The total angular momentum J remains a

conserved quantity but it is not possible to assign a unique overall rotational energy at the transition state, as can be done for vibrator transition states. It is also clear that the quantum number K associated with a symmetric top cannot, in general, be defined for a flexible transition state so that the issue of K being active or adiabatic becomes irrelevant. Note that K does not appear in the density of states expression, equation (32), for flexible transition states. (K associated with overall rotation is not to be confused with k_1, k_2 of the fragments in equation (32)).

In flexible transition state theory (FTST), the rotational energy is most simply expressed in terms of individual fragment rotations and the relative orbital motion [see equation (20)]. For non-rigid molecular systems in which there are free and/or hindered internal rotations, the (instantaneous) overall moments of inertia depend on the relative orientation of the components and the corresponding body-fixed principal axes are not normally aligned with the principal axes of the components. Rotational kinetic energy expressions in which the overall and internal contributions can be simply and separably expressed in terms of constant (orientation-independent) moments of inertia are thus generally not possible. In special cases, such as a rigid frame with 1-d internal rotations which leave the overall moments unchanged (Pitzer and Gwinn 1942) or *orientationally averaged* structures having a higher symmetry than the unaveraged structures (Wardlaw 1982), it becomes possible to assign unambiguously overall and internal rotational energies (if rotation–vibration coupling is neglected). When the rigid frame or averaged structure has a symmetric top, as is often the case, overall rotational energy can be conveniently expressed in terms of J and K. For an averaged structure K must be regarded as an effective or pseudo quantum number whose significance is unknown at present.

3.3. *Vibrator vs. flexible variational transition states*

In section 3.1 vibrator transition states are used for unimolecular reactions with well-defined potential energy barriers. Since many variational transition states are loose, resembling the products, and the Hamiltonian for flexible transition states [equation (20)], has the correct form for the product asymptotic limit, one expects that for these cases flexible transition states to be more accurate than vibrator transition states. However, for some loose transition states the vibrator transition state may be sufficiently accurate or, possibly, even more accurate than the flexible transition state.

One possible inaccuracy in the flexible transition state treatment arises from the classical state counting for the transitional modes, equation (23). However, when tests have been made the quantum correction has been found to be quite small, e.g. $CH_4 \rightarrow H + CH_3$ (Hase, Mondro, Duchovic and Hirst 1987) and $C_2H_6 \rightarrow 2CH_3$ (Klippenstein and Marcus 1987). Implicit in the transitional model Hamiltonian (equation (20)), is the assumption of rigid fragments within which description FTST provides an exact (classical) accounting of the transitional modes. However, as the fragments associate, coupling between the transitional and conserved modes (which is explicitly neglected in FTST) is expected to become increasingly significant. From a normal mode perspective, the transitional modes begin to combine linearly with the vibrational modes of the fragments to form the incipient molecular normal modes of vibration. Closely associated with such coupling is non-rigidity of the fragments. These considerations raise questions about the relative accuracy of equation (20) at small separations but no quantitative assessment has yet been undertaken.

Here the vibrator and flexible treatments of variational transition states are compared for $CH_4 \rightarrow H + CH_3$, $Li^+(H_2O) \rightarrow Li^+ + H_2O$, and $Li^+[(CH_3)_2O] \rightarrow Li^+ + (CH_3)_2O$ dissociation (Zhu *et al.* 1990). The potential energy surface used for these

calculations are described in Hase *et al.* (1987), Mondro *et al.* (1986) and Vande Linde *et al.* (1987), respectively. The values of $k(E, J)$ for the flexible variational transition state treatment are determined as outlined in section 2.2. To locate the transition state and calculate $k(E, J)$ for the vibrator treatment, the transitional modes, whose vibrational frequencies vary along the reaction path, are treated as quantum harmonic oscillators. The 3D/K, active-I model, equation (11), is used to calculate the vibrator $k(E, J)$.

Ratios of vibrator and flexible variational transition state theory rate constants $k(E, J)$, i.e. k_{vib}/k_{flex}, are given in tables 5, 6 and 7 for CH_4, $Li^+(H_2O)$ and $Li^+[(CH_3)_2O]$ dissociation, respectively. The largest value of J considered for CH_4 dissociation is 40 and corresponds to T_r [equation (38)], of 2000 K. For $Li^+(H_2O)$ and $Li^+[(CH_3)_2O]$ dissociation, the largest values J of 80 and 120 correspond to T_r of 2000 and 2100 K, respectively. For $CH_4 \rightarrow H + CH_3$ the $k(E, J)$ values are smaller for the vibrator transition state than for the flexible transition state, with the k_{vib}/k_{flex} ratio nearly equal to unity for small $E(\infty)$. The most probable value for k_{vib}/k_{flex} is approximately 0·8, and its smallest value is nearly 0·5. The ratio k_{vib}/k_{flex} decreases with increase in $E(\infty)$ for small J, but increases with increase in $E(\infty)$ for large J.

For $Li^+(H_2O)$ dissociation the largest difference between the vibrator and flexible transition state $k(E, J)$ values is approximately a factor of two and occurs at the smallest $E(\infty)$. However, in contrast to CH_4 dissociation, here the vibrator transition state $k(E, J)$ is always larger. The k_{vib}/k_{flex} ratio has the same trend at each J for $Li^+(H_2O)$ dissociation. The ratio first decreases with increase in $E(\infty)$ and then slowly increases.

Table 5. Comparison of μCVTST rate constants for $CH_4 \rightarrow H + CH_3$ determined with vibrator and flexible transitions states.

	k_{vib}/k_{flex}				
$E(\infty)$†	$J=0$	$J=10$	$J=20$	$J=30$	$J=40$
0·44	0·944	0·978	–	–	–
0·71	0·781	0·833	–	–	–
1·18	0·754	0·905	–	–	–
1·78	0·647	0·863	0·592	–	–
2·97	0·720	0·810	0·743	–	–
3·57	0·745	0·792	0·751	0·620	–
5·74	0·741	0·814	0·834	0·730	–
5·95	0·726	0·791	0·824	0·713	0·516
7·43	0·731	0·808	0·844	0·739	0·540
8·92	0·738	0·795	0·827	0·798	0·678
9·77	0·715	0·776	0·824	0·767	0·661
11·48	0·715	0·791	0·815	0·786	0·691
12·71	0·709	0·781	0·818	0·795	0·702
15·88	0·705	0·775	0·805	0·793	0·729
19·06	0·723	0·761	0·786	0·799	0·765
20·08	0·719	0·763	0·786	0·803	0·775
24·44	0·715	0·773	0·814	0·847	0·837
29·32	0·717	0·770	0·792	0·811	0·801
34·21	0·720	0·747	0·766	0·820	0·830
39·70	0·702	0·766	0·782	0·820	0·828
47·64	0·704	0·771	0·786	0·818	0·832
55·58	0·707	0·757	0·773	0·813	0·849
63·52	0·707	0·751	0·751	0·769	0·811

† Total energy of the products above their zero-point level.

Table 6. Comparison of μCVTST rate constants for $Li^+(H_2O) \rightarrow Li^+ + H_2O$ determined with vibrator and flexible transition states.

	k_{vib}/k_{flex}				
$E(\infty)$†	$J=0$	$J=20$	$J=40$	$J=60$	$J=80$
0·18	2·13	2·20	2·56	2·46	2·07
0·22	1·89	2·01	2·48	2·52	1·95
0·33	1·85	1·90	2·01	2·17	2·27
0·44	1·71	1·85	1·95	1·98	2·19
0·47	1·76	1·99	1·99	2·12	2·21
0·71	1·52	1·74	1·71	1·78	1·92
0·95	1·41	1·67	1·67	1·70	1·71
1·18	1·40	1·65	1·59	1·41	1·29
1·77	1·36	1·50	1·43	1·39	1·35
2·30	1·32	·142	1·39	1·34	1·28
2·97	1·37	1·43	1·38	1·28	1·25
3·44	1·47	1·44	1·36	1·27	1·26
3·91	1·53	1·46	1·39	1·29	1·23
4·46	1·53	1·50	1·43	1·31	1·19
4·59	1·54	1·48	1·41	1·31	1·27
5·74	1·44	1·49	1·40	1·29	1·20
5·86	1·45	1·51	1·42	1·29	1·17
5·95	1·42	1·49	1·40	1·28	1·17
6·35	1·41	1·47	1·39	1·27	1·21
7·82	1·50	1·46	1·38	1·26	1·16
8·61	1·56	1·47	1·40	1·28	1·20
9·53	1·64	1·53	1·46	1·33	1·21
9·77	1·66	1·55	1·47	1·34	1·19
11·48	1·65	1·57	1·50	1·37	1·20
12·71	1·62	1·59	1·52	1·37	1·23
14·66	1·64	1·62	1·52	1·37	1·23
15·88	1·61	1·61	1·51	1·36	1·24
19·55	1·68	1·63	1·53	1·38	1·22
23·82	1·69	1·68	1·58	1·41	1·24
31·76	1·71	1·71	1·59	1·42	1·26

† Total energy of the products above their zero-point level.

The largest value of k_{vib}/k_{flex} ratio for Li^+ $[(CH_3)_2O]$ dissociation is four and greater than that found for $Li^+(H_2O)$ dissociation. The trend in the rate constant ratio for the lithium cation–dimethyl ether complex at each J is for the ratio to first increase with $E(\infty)$ and then decrease. The smallest values for the rate constant ratio are at the largest J.

The transition state sum of states for $Li^+(H_2O)$ and $Li^+[(CH_3)_2O]$ dissociation does not vary strongly as one moves along the reaction path. Thus, since the sum of states for the flexible variational transition state is derived in part by a Monte Carlo method with an associated numerical uncertainty, there is a resulting uncertainty of about ± 1 Å in the position of the minimum in the flexible variational transition state sum of states for these ion-molecule dissociations. In contrast, the minimum in the transition state sum of states is well localized for CH_4 dissociation. As a result, a comparison is meaningful between the positions of the vibrator and flexible variational transition states along the reaction path. This comparison is given in figure 6, where the C–H distance is plotted for the vibrator and flexible transition state models. It is seen that these two models give similar transition states.

Table 7. Comparison of μCVTST rate constants for $Li^+[(CH_3)_2O] \rightarrow Li^+ + (CH_3)_2O$ determined with vibrator and flexible transition states.

	k_{vib}/k_{flex}				
$E(\infty)$†	$J=0$	$J=30$	$J=60$	$J=90$	$J=120$
0·21	2·10	2·33	2·16	1·88	1·28
0·29	2·18	2·40	2·22	1·93	1·54
0·43	2·36	2·55	2·36	2·05	1·54
0·72	2·83	2·99	2·79	2·45	1·91
1·09	3·38	3·91	3·54	2·66	1·65
1·35	3·41	3·82	3·48	2·66	1·71
2·03	3·63	3·87	3·55	2·78	1·92
2·70	3·85	4·11	3·70	2·65	1·56
3·31	3·78	4·05	3·65	2·67	1·66
4·71	3·66	3·95	3·64	2·76	1·79
5·07	3·71	4·00	3·69	2·82	1·85
6·47	3·78	4·01	3·75	2·93	1·99
7·06	3·78	4·00	3·75	2·96	2·05
8·28	3·58	3·78	3·45	2·50	1·51
9·71	3·56	3·75	3·45	2·54	1·56
12·42	3·48	3·62	3·37	2·57	1·69
17·65	3·28	3·39	3·14	2·36	1·55
21·86	3·28	3·40	3·18	2·45	1·64
24·26	3·25	3·26	3·06	2·41	1·72
29·73	3·25	3·20	2·96	2·27	1·55

† Total energy of the products above their zero-point level.

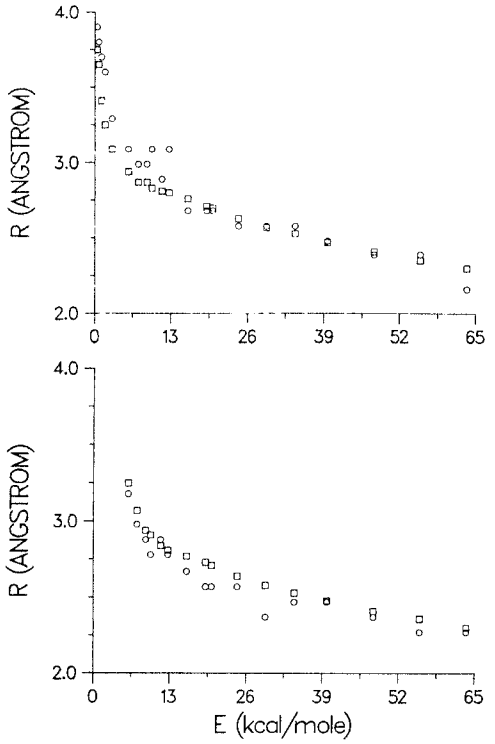

Figure 6. Plots of the vibrator (○) and flexible (□) variational transition state theory values of the H–CH_3 bond distance at the transition state: upper, $J=0$; lower, $J=40$.

4. Angular momentum and thermal unimolecular rate coefficients

The rate of collision-induced gas phase decomposition of a species in excess buffer gas, M, generally depends on temperature, T, and pressure, $[M]$. In the high pressure limit the rate becomes independent of $[M]$ and the overall rate coefficient reduces to a Boltzmann average of microcanonical rate coefficients, viz.

$$\lim_{[M]\to\infty} k(T,[M]) = k(T) = \sum_{J=0}^{\infty} \int dE \frac{N(E,J)}{Q_r(T)} \exp(E/k_B T)\, k(E,J)$$
$$= \frac{1}{hQ_r(T)} \left[\sum_{J=0}^{\infty} \int dE G(E,J) \exp(-E/k_B T) \right]. \tag{39}$$

The J-dependence of $k(T)$ is carried by $G(E,J)$ and $Q_r(T)$, the reactant partition function. When $G(E,J)$ is determined variationally for each (E,J) pair one obtains a 'microcanonical' variational thermal rate coefficient, denoted $k_\mu(T)$. When the quantity in square brackets is determined first and then minimized, one obtains a 'canonical' thermal rate coefficient, denoted $k_c(T)$. If the transition state location is independent of E and J, $k_\mu = k_c$, as would approximately be the case for a dissociation reaction having a large potential barrier on the reaction path, e.g. $H_2CO \rightarrow H_2 + CO$. In SACM, $k_\mu(T)$ is obtained by setting $G(E,J)$ in equation (39) to the number of open adiabatic channels.

At lower buffer gas pressures theoretical models should, in principle, also account for the J-dependence of intermolecular energy transfer in collisions between the reactant and buffer gas. The importance of including J-dependent energy transfer probabilities and conservation of angular momentum in the fall-off and low pressure regimes has been stressed in a recent master equation treatment of unimolecular and recombination reactions (Smith and Gilbert 1988). Via analytic parameterization of master equation solutions, simplified statistical rate coefficient models have been developed for these regimes (Troe 1977, 1979, Gilbert, Luther and Troe 1983). These models are capable of incorporating angular momentum effects in a modified strong collision approximation with or without weak coupling correction. Such a model was used, in conjunction with FTST, to represent an extensive set of recombination rate coefficients for methyl radical self recombination (Wagner and Wardlaw 1988). Although direct experimental studies (e.g. Hippler, Troe and Wendelken 1983) and classical trajectory studies (e.g. Bruehl and Schatz 1988) of average energy transfer $\langle \Delta E \rangle$ have provided valuable insight into factors affecting this quantity, much remains to be learned about the dependence of this process on angular momentum.

In the high pressure limit where dissociation is effectively unimolecular it is relatively easy, from a theoretical point of view, to examine the role of angular momentum. We do so using the results of several versions of VTST as applied to a few neutral–neutral and ion–molecule recombination reactions. (Transition states for recombination reactions are the same as for the reverse unimolecular process.) Of practical interest are comparisons of microcanonical versus canonical versions of $k(T)$, and of separable versus non-separable treatments of the transitional modes in CVTST. To emphasize the diversity in the dependence of transition state locations on E and J when there is no barrier to recombination, we present contour plots of $R^\ddagger(E,J)$, as determined by μFTST, for three reactions. For $CH_3 + H \rightarrow CH_4$ (figure 7) the dependence of $R^\ddagger$ on J is seen to be weak, whereas $R^\ddagger$ decreases with increasing E, as is typical of barrierless association reactions. The same behaviour is observed for $2CH_3 \rightarrow C_2H_6$. Such a weak dependence on J can be exploited to reduce the

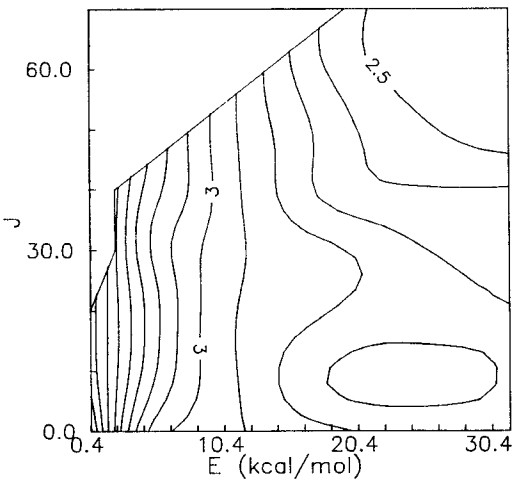

Figure 7. Contours of transition state location $R^{\ddagger}$ as a function of E and J (units of $\hbar$) for $CH_3+H\rightarrow CH_4$, obtained using μFTST. The energy is measured with respect to $V(\infty)$ + zero point energy of the isolated fragments. The fine details of the plot are not important, since there is an uncertainty in $R^{\ddagger}$ of about 0·1 Å. The blank region in the upper left-hand corner is where E is less than the effective potential. The contour is 0·1 Å.

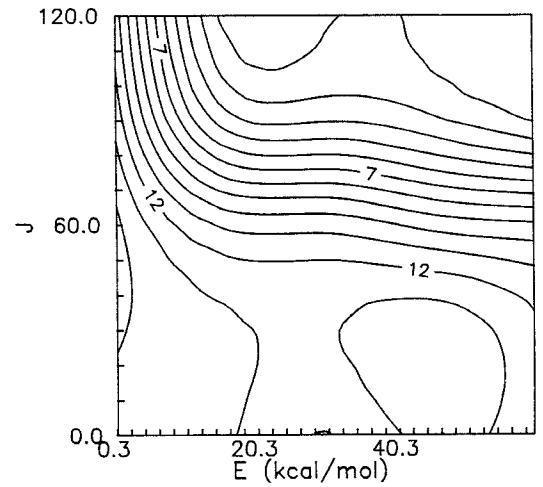

Figure 8. Same as figure 7 but for $Li^+ + H_2O\rightarrow Li^+(H_2O)$, with an uncertainty in $R^{\ddagger}$ of about 1 Å and with a contour increment of 1 Å.

computational effort in μVTST applications: one only needs to minimize $G(E)=\Sigma_J G(E,J)$ with respect to the reaction coordinate for a set of E values, rather than minimize $G(E,J)$ on grid of (E,J) values. Song and Chesnavich (1989, 1990) have invoked this approximation in their modification of FTST for triatomic reactants and have verified it for $HO_2\rightarrow OH+O$ and $HeH_2^+\rightarrow HeH^+ + H$. In sharp contrast is the $Li^+ + H_2O\rightarrow Li^+(H_2O)$ reaction (figure 8), for which the E-dependence of $R^{\ddagger}$ is generally weak, $R^{\ddagger}$ is almost constant for $J<60$ but decreases rapidly as J increases beyond 60, and the range of $R^{\ddagger}$ values (2–14 Å) is much greater than for CH_3+H. The contour diagram for another ion–molecule system, $Li^+ + (CH_3)_2O\rightarrow Li^+(CH_3)_2O$ (figure 9), provides an example of an intermediate case where $R^{\ddagger}$ depends strongly on both E and J. It has been found (Aubanel and Wardlaw 1990) that the gross features of

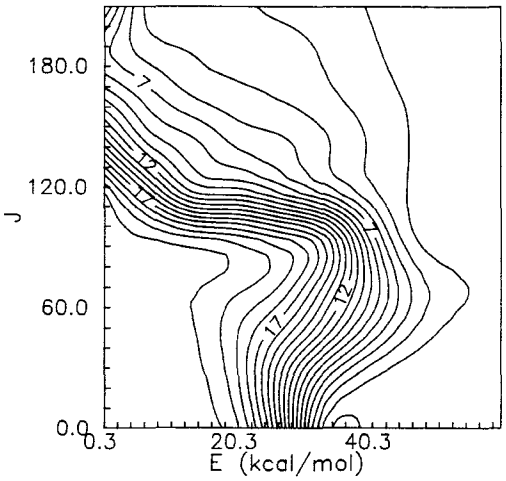

Figure 9. Same as figure 8 but for $Li^+ + (CH_3)_2O \rightarrow Li(CH_3)_2O$, with an uncertainty in $R^\ddagger$ of about 3 Å.

the J-dependence of the transition state locations for these three systems (*a*) can be rationalized by a simple analysis of the location and occurrence of centrifugal barriers in the effective potential along the reaction coordinate, and (*b*) are in qualitative agreement with the predictions of a simple μVTST model for $G(E, J)$ in which the pseudo-diatomic approximation is made for overall rotation (Hase and Wardlaw 1989, Hase and Hu 1989, Hu and Hase 1989).

It is of interest to assess the influence of this varied $R^\ddagger$ behaviour and of angular momentum conservation on the accuracy of the widely applied CVTST which offers the convenience of a *single* minimization of the quantity in square brackets in equation (39) at each temperature. Since the preferred μVTST requires minimization for each (E, J) pair, it tends to be computationally intensive and is often avoided. Theoretical thermal rate coefficients for $CH_3 + H \rightarrow CH_4$, $Li^+H_2O \rightarrow Li^+(H_2O)$, and $Li^+ + (CH_3)_2O \rightarrow Li^+(CH_3)_2O$ are plotted in figures 10–12, respectively. We first compare FTST evaluations of k_μ and k_c. Angular momentum conservation is rigorously treated in each case and the two rate coefficients differ only in the application of the variational principle, as is discussed following equation (39). As expected, $k_\mu < k_c$ in each case, since $G(E, J, R) \geqslant G(E, J, R^\ddagger)$. However, for $CH_3 + H$, k_c is 5–10% larger than k_μ (300–2500 K), which is to be contrasted with 20–50% for $Li^+ + H_2O$ (200–1000 K), and $\sim 55\%$ for $Li^+ + (CH_3)_2O$ (200–1000 K). For $CH_3 + H$ the (small) discrepancy between k_μ and k_c is primarily attributable to the neglect of the E-dependence of $R^\ddagger$ in determining k_c; the J-dependence of $R^\ddagger$ is rather weak (see figure 7). For the ion–molecule reactions the J-dependence of $R^\ddagger$ is strong and $R^\ddagger$ varies over much larger ranges than has been observed for free radical association reactions. This is attributable to the stronger long-range intermolecular potential between an ion and a molecule. Consequently, CVTST is less accurate with both the E-dependence and the J-dependence of $R^\ddagger$ contributing to the discrepancy between k_μ and k_c. Also plotted in figures 10–12 is a CVTST rate coefficient, denoted k'_c, obtained by treating the (two) transitional modes in each system as a classical 2-d hindered rotor. On the 200–1000 K temperature range $k_c \approx k'_c$ for $CH_3 + H$, whereas k'_c is $\sim 15\%$ larger and $\sim 25\%$ larger than k_c for $Li^+ + H_2O$ and $Li^+ + (CH_3)_2O$, respectively. These two rate coefficients are expected to be similar since each results from a treatment in which no approximation is made to the transitional mode potential. The major difference between the two methods is that in CFTST (k_c)

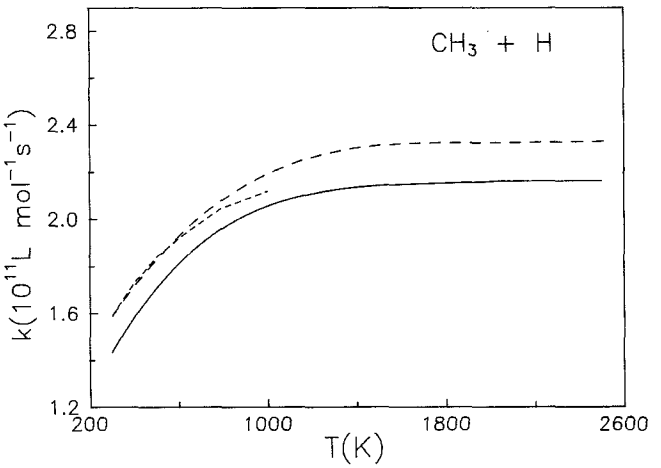

Figure 10. Theoretical rate constants for $CH_3+H\rightarrow CH_4$: k_μ(——), k_c(– – –), k'_c(- - -), as defined in the text.

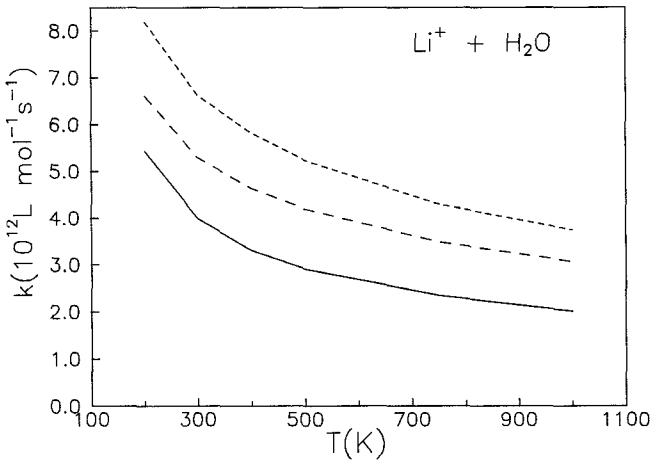

Figure 11. Same as figure 10 but for $Li^+ + H_2O \rightarrow Li^+(H_2O)$.

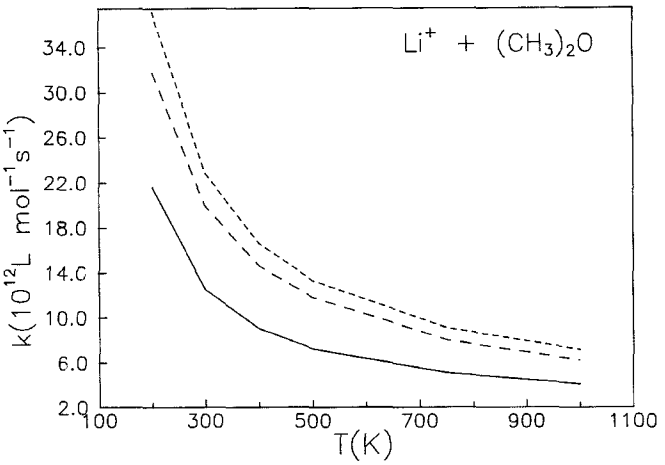

Figure 12. Same as figure 10 but for $Li^+ + (CH_3)_2O \rightarrow Li^+(CH_3)_2O$.

energy and angular momentum conservation are rigorously included, whereas in the CVTST of Hase *et al.* (k'_c) a transitional mode partition function is obtained by assuming *complete separability* of the transitional modes from overall rotation. It seems reasonable to assume that some of the discrepancy between k_c and k'_c for the two ion-molecular systems is attributable to neglect of angular momentum conservation in the separable CVTST model.

5. Vibrational/rotational adiabatic theory

The implications of adiabaticity of (fast) motion in coordinates orthognal to the reaction coordinate (along which the motion is presumed relatively slow) for the validity of traditional transition state theory were first investigated about 50 years ago (Hirschfelder and Wigner 1939) but it was 20–30 years before development of so-called adiabatic transition state theory occurred (e.g. Eliason and Hirschfelder 1959, Hofacher 1963, Marcus 1966). The utility of an adiabatic theory of chemical reactions is twofold. First, it can, under suitable circumstances (system type, initial conditions), provide a reasonably accurate description of the bimolecular reaction dynamics. Second, adiabatic theory provides a basis for a class of statistical models for unimolecular rate coefficients and product properties. It is the latter application which concerns us here.

The implementation of a statistical vibration/rotation adiabatic model is, from a formal perspective, straightforward. Practical limitations and ensuing approximate implementations are discussed separately below. As in transition state theory, the reaction coordinate R is assumed separable from the remaining degrees of freedom. For a given E and J and for each value of R the rovibrational eigenvalues $E_a(R)$ are obtained. For states of a given symmetry type, the result is a set of non-intersecting curves, commonly called adiabatic channel curves, which smoothly connect reactant ($R=R_e$) and product ($R\to\infty$) rovibrational energy levels. Each $E_a(R)$ curve has a maximum E_a^{max} at $R=R_a^{max}$, $R_e\leqslant R_a^{max}\leqslant\infty$, and each correlates a reactant energy level to a particular product energy level. Conservation of J is implicit in this procedure. Open adiabatic channel curves are those having $E_a^{max}<E$ and the number of such channels is here denoted as $G_a(E,J)$. The statistical adiabatic rate coefficient.

$$k_a(E,J)=\frac{G_a(E,J)}{hN(E,J)} \tag{40}$$

is analogous to the corresponding RRKM theory expression [equation (16)]. The 'transition state' of statistical adiabatic theory is, for given E and J, delocalized as it is associated with a set of R_a^{max} values (Quack and Troe 1981). This is to be contrasted with RRKM theory in which the transition state location $R^{\ddagger}$ is fixed for given E and J. The energy levels E_a^{max} can be used to construct a transition state type pseudo-partition function if a canonical implementation of the theory is desired.

If the intramolecular dynamics of the energized reactant were truly adiabatic, each molecular rotational/vibrational state would have a unique individual molecular rate constant and would decompose to distinct product states. Many experiments and the broad applicability of RRKM theory illustrate that many unimolecular processes do not behave in this manner. Thus, two statistical postulates, analogous to those of transition state theory, are invoked to obtain equation (40) from the formalism of resonance scattering theory (Quack and Troe 1974). First, it is assumed that all reactant states in the range $(E, E+\mathrm{d}E)$ are equally and strongly coupled to a particular open (i.e. one with $E>E_a^{max}$) product channel; closed product channels are assumed to be weakly coupled to reactant states. Second, all open product channels are equally

probable and have unit transmission probability. The physical implications (Quack and Troe 1981) of these assumptions are the following: within the strong coupling region, as defined by the locations $\{R_a^{max}\}$ of the adiabatic channel maxima, the dynamics is decidedly non-adiabatic and leads to a quasi-microcanonical distribution of reactant states. Beyond the strong coupling region, the dynamics is strictly adiabatic and no transitions between channels occur. The latter implication is in general unrealistic, particularly for channels having maxima near R_e and for systems with highly anisotropic long-range potentials (Quack and Troe 1981). The inclusion of exit channel effects in the prediction of product properties is discussed in section 6. The spirit of statistical adiabatic theory is that it provides a potentially reliable way of counting product states accessible from reactants in the absence of severe deviations form adiabaticity outside the strong coupling region. The effect of non-adiabaticity is expected to be greatest near threshold where only a small number of channels is open.

Determination of rovibrational energy levels on a range of R values requires a global potential energy function. These remain generally unavailable although potentials based on *ab initio* calculations now exist for a small but increasing number of intensely studied reactive systems. In any case, obtaining the quantum eigenvalues at all relevant values of R is clearly not feasible despite continuing improvements in computing technology. In order to proceed with this type of model it is necessary to introduce further approximations.

The most well known and widely used such treatment is the statistical adiabatic channel model (SACM) which provides an approximate prescription for calculating the number of open channels and hence $G_a(E, J)$ (Quack and Troe 1974). It is assumed that the rovibrational eigenvalues can be modelled at any R value via an exponential function

$$g(R) = \exp[-\alpha(R - R_e)] \tag{41}$$

which interpolates between reactant ($R = R_e$) and product ($R \to \infty$) eigenvalues:

$$E_a(R) = E_a(n_p, \infty) + [E_a(n_r, R_e) - E_a(n_p, \infty)]g(R) + E_{cent}(R) + V(R), \tag{42}$$

where $V(R)$ is the potential energy along the reaction coordinate; n_p and n_r denote the totality of internal quantum numbers for motion orthogonal to R for product fragments and the reactant molecule, respectively; $E_{cent} = P(P+1)/2\bar{I}(R)$ is a centrifugal term with $P = l + (J - l)g(R)$, l is the orbital angular momentum of the fragments and $\bar{I}(R)$ is an R-dependent, approximate moment of inertia. The potential energy surface is thus parameterized, in the intermediate region, by a single parameter α which is treated as adjustable. In fitting SACM to *thermal* rate data it was found (Cobos and Troe 1985) that $\alpha = 1{\cdot}0 \pm 0{\cdot}2$ Å^{-1} described 18 of 26 systems to which a simplified version of SACM was applied. The eigenvalues $E_a(n_p, \infty)$ and $E_a(n_r, R_e)$ are usually determined via rigid rotor and harmonic/Morse oscillator models of the reactant and product internal degrees of freedom.

The reactant–product correlation $n_r \to (n_p, l)$ in equation (42) is achieved by pairing successively higher energy levels of reactant and product beginning with the lowest energy state for each J and subject to the following restrictions: (i) angular momentum coupling constraints (i.e. $|J - J_r| \leqslant l \leqslant J + J_r$, where J_r is defined by equation (22)), and (ii) adiabaticity of the conserved vibrational modes (their vibrational quantum numbers are independent of R). The latter restriction, although physically unrealistic in general, considerably simplifies the correlation scheme, particularly for larger polytomics. A futher restriction is the correlation of only those states of the same symmetry.

In practice all states are correlated regardless of symmetry and $G_a(E,J)$ is then multiplied by an approximate symmetry correction factor. This is reasonable for energies sufficiently in excess of the reaction threshold energy (Miller 1983).

Despite the aforementioned simplifications, direct numerical count for $G_a(E,J)$ becomes too cumbersome for large molecules because of the large number of energy levels to be correlated and the correspondingly large number of channel maxima to be located (usually numerically). Subsequent to the original version of SACM (Quack and Troe 1974), various additional approximations have been introduced to simplify the calculation of rate coefficients within the SACM framework. Several simplification schemes are outlined below with reference to the treatment of angular momentum. In the earliest such approach (Quack and Troe 1977), thermal rate coefficients $k(T)$ were obtained via a maximum free energy criterion. Instead of interpolating between reactant and product eigenvalues to obtain adiabatic channel curves, the total free energy was interpolated using a function of the same form as equation (41). Conservation of total angular momentum is sacrificed in favour of the convenience of a separable pseudo-partition function $Q^* = \Sigma_a \exp[-E_a^{max}/kT]$. The corresponding approach to $k(E,J)$ would involve interpolating $G_a(E,J)$ between reactant and product limits and applying a minimum number of states criterion. In a rather different approach (Troe 1981, 1983) the channel coordinates are assumed separable (initially) in their contribution to the channel threshold energy E_a^{max}. For a represenative system the pattern of threshold energies for each type of coordinate (i.e. conserved and transitional) was analysed, for $J=0$, and then modelled by an *ad hoc* empirical expression. Convolution of the individual sums of states provides the approximate quantity $G_a^0(E,J=0)$. For $J \neq 0$, $G_a^0(E,J)$ is obtained from $G_a^0(E,J=0)$ by displacement of the energy scale, $E \rightarrow E - E_0(J)$, where $E_0(J)$ is a centrifugal barrier height. Several *a posteriori* corrections are then applied, including an angular momentum factor which compensates for the violation of angular momentum coupling constaints imposed by the separation of coordinates. This factor is represented as an interpolation between reactant and product correction factors which are readily evaluated. In a recent approach (Troe 1987), designed for ion–molecule capture processes at low temperatures, adiabatic channel curves are determined analytically by perturbation theory or series expansion applied to the long-range potential. These curves are functions of j (the molecular rotation quantum number) and l (the orbital quantum number) where $\boldsymbol{j}+\boldsymbol{l}=\boldsymbol{J}$.

6. Angular momentum distribution for non-thermal unimolecular reactions

The distribution of angular momentum for the unimolecular reactant depends on the excitation process. Excitation by electromagnetic radiation can result either in broad or narrow angular momentum distributions. The form of this distribution depends on the temperature of the unexcited reactants and the resolution of the excitation process. In local mode overtone excitation (Crim 1984), such as CH bond excitation in CH_3N (Reddy and Berry 1977), the unexcited reactants usually have a room temperature Boltzman distribution of rotational energies. If the transition moments are the same for the unexcited reactant J-, K-levels, which is usually a good approximation, this rotational energy distribution will be projected on to the vibrationally excited reactant. Thus, the reagent rotational temperature is the principal determinant of the excited reactant's angular momentum distribution.

Reactants excited to a specific J-, K-level have been prepared by a two-photon process called simulated emission pumping (SEP) (Kittrell *et al.* 1981). The first laser prepares a vibrational level of an excited electronic state. Before this state undergoes a spontaneous radiative or non-radiative transition, a second laser with a lower energy photon stimulates emission of light and the formation of a highly excited level of the ground electronic state. Because of the high resolution of the lasers, individual rotation-vibration states may often be prepared. An infrared-optical double resonance technique has also been used to prepare specific J-, K-levels for an excited reactant on the ground potential energy surface (Rizzo 1990).

A widely used excitation process, but one for which the angular momentum distribution of the excited reactant is not well understood, is chemical activation. Here, collision complexes are formed by processes such as $H+C_2H_4 \rightarrow C_2H_5$ (Hase *et al.* 1983), and $Cl^- + CH_3Cl \rightarrow Cl^- - CH_3Cl$ (Vande Linde and Hase 1990). The distribution of the total angular momentum J for the collision complex depends on the rotational angular momentum j_a and j_b for the collision partners, the collision orbital angular momentum l, and the 'stereochemistry' associated with the addition of the $\boldsymbol{j}_a$, $\boldsymbol{j}_b$ and $\boldsymbol{l}$ vectors in forming the total angular momentum vector $\boldsymbol{J}$, i.e. $\boldsymbol{J}=\boldsymbol{j}_a+\boldsymbol{j}_b+\boldsymbol{l}$.

The most understood situation occurs when the rotational angular momenta of the collision partners are zero. Thus, the rotational angular momentum distribution of the collision complex is simply the distribution of orbital angular momentum which leads to complex formation. Classically, the orbital angular momentum is defined in terms of reactant relative translational velocity v_t and the collision impact parameter b, and is given by $l=\mu b v_t$. The probability a collision has a particular value of l is $P(l)=2l^2/l_m^2$. Therefore, if the collision partners have no rotational angular momentum, the probability of J is simply the product of $P(l)$ and the probability $P_c(l)$ of complex formation at l, i.e.

$$P(J)=2P_c(l)\frac{l^2}{l_m^2}. \tag{43}$$

To determine the projection of J on to the collision complex and, thus, K for a symmetric top, the preferred orientations of the collision-partners as they react must be understood (Parson *et al.* 1973). Distributions of angular momentum have been determined for random (i.e. purely statistical) orientations of the reacting collision partners (Miller *et al.* 1967, Chesnavich and Bowers 1977b, 1979). For collisions between two diatomics, such statistical distributions have been evaluated and compared to the actual distributions obtained from ensembles of classical trajectories (Wardlaw 1982).

The association dynamics becomes considerably more complex if the collision partners have rotational angular momentum. However, the problem is simplified if one of the collision partners is an atom (or has zero rotational angular momentum) so that the total angular momentum becomes $\boldsymbol{J}=\boldsymbol{l}+\boldsymbol{j}$. If $\boldsymbol{l}$ and $\boldsymbol{j}$ add randomly in forming the collision complex, the probability of J (Hase and Wolf 1981) is

$$P_{l,j}(J)=\frac{2J}{|l+j|^2-|l-j|^2}. \tag{44}$$

For most reactions it is doubtful that l and j add randomly. As described above, there are often preferred orientations for the collision partners. Thus, if j and its projection k are specified for the reactant, there will be a non-random distribution of $\boldsymbol{l}+\boldsymbol{j}$ vector sums for the collision complex. Also, it has been speculated that on dynamical grounds

it may be difficult for a collision complex to accommodate a large value of J. For the H+C=C→H–C–C model system, it was found (Hase and Wolf 1981) that as j for C=C is increased H–C–C complexes are preferentially formed from collisions with $l+j$ angles less than 90°, which results in an average J value smaller than the random (i.e. statistical) value.

Overall, very little is known regarding the manner in which the orbital and rotational angular momentum vectors add in forming the total angular momentum of a collision complex. However, to calculate accurate RRKM rate constants for collision complexes the distribution of J must be known as well as the distribution for the projection of J on to the complexes' symmetry axis. This is an area of research, concerning angular momentum in unimolecular rate theory, where much more work needs to be done.

7. Product properties

A description of unimolecular processes complementary to that provided by average rate coefficients for decomposition to a particular product arrangement is provided by product property distributions within that arrangement. A complete list of such properties is extensive and includes vibrational, rotational and translational energies, various angular momenta, and the relative orientation of pairs of vector quantities, e.g. the angle between two angular momentum vectors. To simplify discussion and focus attention on the ideas behind various models for product properties, we shall consider only product rotation and vibration. Furthermore it is rotational/vibrational quantum number distributions which have been measured directly in recent photodecomposition experiments on hydrogen peroxide (Rizzo *et al.* 1984, Ticih *et al.* 1986, Brouwer *et al.* 1987), nitrosyl cyanide (Noble *et al.* 1984, Nadler *et al.* 1985, Qian *et al.* 1985, Klippenstein *et al.* 1988) and ketane (Green *et al.* 1988, Klippenstein and Marcus 1989). In each case experimentally derived distributions were compared to a statistical distribution derived from variational RRKM theory, phase space theory or the statistical adiabatic channel model. The reader is referred to the individual papers and to a review by one of us (Wardlaw and Marcus 1988) for analyses of several of these comparisons between theory and experiment.

Little is known about the dependence of product properties on J since in most experimental studies, including those cited above, a thermal distribution over J was unavoidable. Current experiments (Rizzo 1990), which provide OH rotational quantum number distributions resulting from decomposition of a *particular* (J, K) rotational state of H_2O_2, offer the first opportunity for assessing J-dependence of product internal energy distributions.

The relative population of product states with energy E_i in internal mode i is

$$P(E, J; E_i) = \frac{F(E, J; E_i)}{F(E, J)}, \tag{45}$$

where $F(E, J)$ is the total number of quantum states accessible to the *dissociated* system for the given (E, J), and $F(E, J; E_i)$ is the corresponding number of accessible states having energy E_i in mode i (Quack and Troe 1975). Each of the three models mentioned earlier and described briefly below relies directly or indirectly on $G(E, J)$ to obtain $F(E, J)$ and $F(E, J; E_i)$, and hence $P(E, J; E_i)$. As such, explicit treatment of the total angular momentum is not required since the sum of states G already accounts, in principle, for conservation of this quantity.

7.1. *SACM*

Since all 'open' channels are assumed to be populated with equal weight and all reactant and product states are correlated, product properties follow trivially:

$$P(E, J; E_i) = G_a(E, J; E_i)/G_a(E, J). \tag{46}$$

The effort of this approach is concentrated in the correlation process and in the determination of the number of channels open at the given E (Quack and Troe 1975).

7.2. *Phase space theory*

In this widely applied model, all product states are assumed to be populated with equal probability subject to the constraints that (*a*) the orbital angular momentum is less than a critical value (determined by E and the long-range potential) above which the separating fragments cannot surmount the centrifugal barrier, and (*b*) total angular momentum is conserved. The former constraint makes phase space theory formally equivalent to loose transition state theory wherein the transition state is located at the top of the centrifugal barrier. As such, the only 'exit channel' effect is a coupling between translation along the relative separation coordinate and orbital motion of the fragments; all orbital rotational energy at the transition state is converted to relative translational energy of the products. For such systems several related (classical) models for the translational energy distribution of separated products are available (Safron 1972, Holmlid and Rynefors 1977, Wardlaw 1982). The simplicity of these models relative to rigorous application of phase space theory is attributable to an approximate treatment of angular momentum conservation.

7.3. *Variational RRKM theory*

A wide range of transition state locations is found in the application of variational transition state theory to dissociation reactions having no barrier to the reverse process of association. Accordingly one must, in the general case, allow for the influence of exit channel couplings in order to predict the properties of separated products based on the transition state distributions embodied in $G(E, J)$. Two ways to accomplish this in approximate fashion are outlined below. One models the effect of exit channel dynamics within the framework of FTST and the other handles the exit channel dynamics explicitly using classical trajectories.

7.3.1. *FTST model*

A model for product vibrational and rotational distributions based on VTST was introduced by Wardlaw and Marcus (1988). Subsequently Marcus (1988) constructed a refined version which successfully describes rotational quantum number distributions of products arising from the decomposition of NCNO (Klippenstein *et al.* 1988) and CH_2CO (Klippenstein and Marcus 1989). It is the latter model which we describe here. The conserved modes are assumed vibrationally adiabatic (as in SACM) after passage through the transition state and, consequently, the distribution of vibrational quantum numbers for the products is that at the transition state. The transitional modes are assumed non-adiabatic between the variationally determined transition state and a loose transition state determined by the orbital angular momentum l and the radial potential. Beyond this loose transition state the transitional modes are treated as adiabatic. For energies below those needed to yield vibrationally excited products, the

phase space theory distribution of product rotational states is obtained. At energies above the vibrational excitation thresholds, the product rotational state distributions are generally expected to differ from those of phase space theory.

7.3.2. *Trajectory model*

RRKM theory assumes that the relaxation dynamics of the molecule is sufficiently rapid to maintain a microcanonical distribution of states at the transition state. Trajectory initial conditions could, in principle, be selected uniformly from this transition state distribution and an ensemble of trajectories propagated to the product region, provided that the potential energy surface from the transition state region to the asymptotic region is available. Product property distributions would then be readily extracted from the trajectory final conditions. Such an approach is difficult to implement in general, because of the complexities of sampling from a microcanonical distribution in a region intermediate between reactant and product. It has however been applied to a 3-atom system in a study of post barrier effects on energy exchange (Rynefors 1982). An alternative approach has been proposed by Hamilton and Brumer (1985) who choose to initiate a microcanonical set of trajectories in the *product* region and propagating this ensemble towards the parent molecule. The initial conditions for these 'time reversed' trajectories are readily determined via standard quasi-classical techniques and represent a phase space theory distribution. One retains those trajectories which reach a (predetermined) transition state and discards the remainder, leaving an 'exit channel corrected' ensemble which is implicitly assumed to correspond to a microcanonical distribution at the transition state. Product internal energy distributions are then extracted from this corrected phase space theory set of trajectory initial conditions. The well-known problem of violation of zero point energy conservation by classical trajectories (Bowman *et al.* 1989, Miller *et al.* 1989) is ignored in this model, although it is not expected to be a serious one for the direct processes (i.e. short-time dynamics) involved here.

8. Conclusions

8.1. *Summary*

In this review we have given a historical perspective of various treatments of angular momentum, as used in statistical rate theories to calculate attributes of unimolecular reactions. RRKM, phase space, and statistical adiabatic rate theories are considered. The treatment of angular momentum in RRKM theory is reviewed for both vibrator and flexible transition states. The latter type of transition state is particulary important for simple bond dissociation reactions without saddle points. Several illustrative applications of RRKM theory are given.

For the most part, in calculating RRKM unimolecular rate constants for vibrator transition states the vibrational and rotational motions have been assumed separable. Diatomic, and K-active and K-adiabatic symmetric top models have been used to represent the rotational kinetic energy. One K-active model includes a vibrational–rotational coupling effect. These different models may yield considerably different $k(E, J)$ unimolecular rate constants, e.g. tables 2–4.

The treatment of the angular momentum associated with flexible transition states for unimolecular bond ruptures and ion-molecule dissociations such as $CH_4 \rightarrow H + CH_3$ and $Li^+(H_2O) \rightarrow Li^+ + H_2O$ is reviewed. For ion-molecule reactions a traditional approach has been to place the flexible transition state at the centrifugal

barrier, i.e. an orbiting transition state. In a more complete analysis one should consider the anisotropy of the long-range intermolecular potential for the dissociating fragments and use variational RRKM theory to calculate the transition state structure as a function of E and J. In the variational flexible transition state approach of Wardlaw and Marcus (1988), the angular momenta for the individual fragments, for the relative orbital motion, and for external rotation are correctly coupled. This approach is compared with more approximate methods of calculating high pressure thermal unimolecular rate constants.

Both vibrator and flexible transition states have been used to calculate variational RRKM $k(E, J)$ unimolecular rate constants. These two approaches are compared here for $CH_4 \rightarrow H + CH_3$, $Li^+(H_2O)$, and $Li^+[(CH_3)_2O] \rightarrow Li^+ + (CH_3)_2O$ dissociations. The difference between the vibrator and flexible transition state $k(E, J)$'s decreases as J is increased for ion–molecule dissociations. This is not a pronounced effect for methane dissociation.

A brief description is given of statistical adiabatic theory for calculating unimolecular rate constants and product energy partitionings. Approximate procedures for calculating the adiabatic potential energy curves and counting the number of open channels are considered. Additional assumptions are usually required to calculate product energy distributions from RRKM theory. If the transition state is located at the centrifugal barrier, the only additional assumption is that orbital angular momentum is conserved between the transition state and products. For vibrator or flexible transition states located inside the centrifugal barrier, different postulates can be made regarding the degree of non-adiabaticity and coupling between vibrational and rotational degrees of freedom as the reactive system proceeds from the transition state to products. Classical trajectories can be used to provide a dynamical treatment of this non-adiabatic coupling.

There is currently an incomplete understanding of the form of the angular momentum distribution for unimolecular reactants prepared by chemical activation, e.g. $F + C_2H_4 \rightarrow C_2H_4F$. This distribution is affected by the anisotropy of the reagent intermolecular potential and dynamical correlations between the reagent orbital and rotational angular momenta. Another outstanding issue, considered below, is the treatment and significance of vibrational–rotational coupling in unimolecular rate theory.

8.2. *Rotation–vibration coupling*

The coupling between rotation and vibration enters unimolecular rate theory in two ways. First, it influences the dynamics of intramolecular energy transfer whose relative rapidity is central to the validity of statistical models. Recent experimental studies (e.g., Rizzo 1990, Farley *et al.* 1988) and theoretical studies (e.g., Sahm and Uzer 1989, Shirts 1987, Ezra 1986, Uzer *et al.* 1985) are beginning to probe the role of rotation in the energy redistribution process. Second, such a coupling influences energy levels and hence sums and densities of state which in turn determine the RRKM rate coefficient. Of these two aspects, we shall consider only the latter; the former, although of fundamental importance, is deemed to lie beyond the scope of this review.

The absolute and relative values of rovibrational energy levels in a separable treatment of these two types of motion will generally differ from the corresponding values in a treatment which accounts for rotation–vibration coupling. Although the strength of such a coupling is expected to increase with J at least for small and intermediate J, little is known about the associated J-dependence of energy level

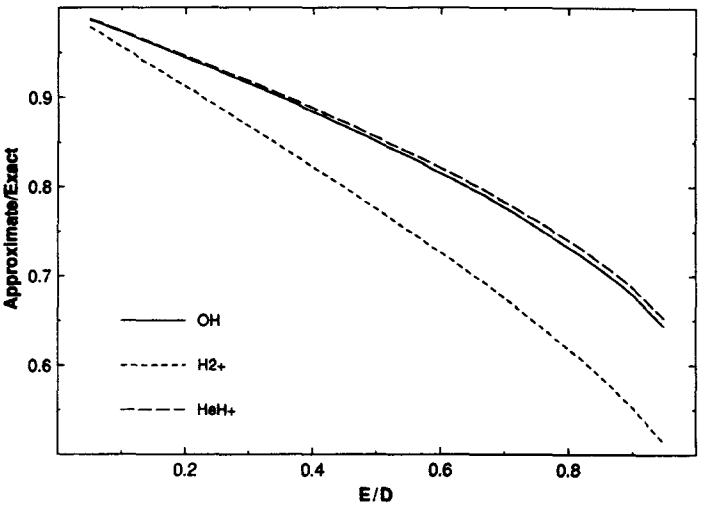

Figure 13. Ratio of the approximate (assuming separation of vibration and rotation) to exact classical sum of states for a rotating Morse oscillator.

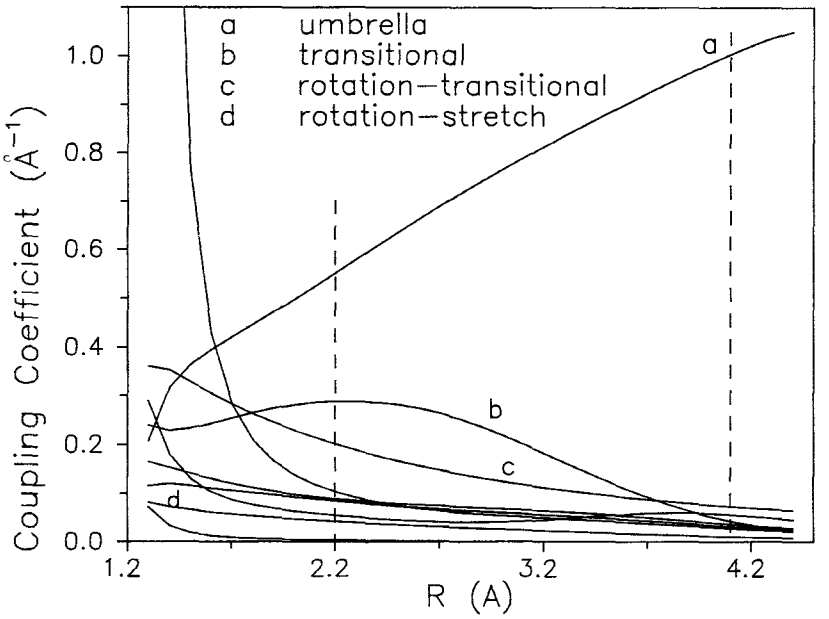

Figure 14. Coupling coefficients as a function of the C–H separation R for $CH_3 + H \rightarrow CH_4$. The transition state region is located between the dashed lines.

patterns. Both the density of states (reactant) and sum of states (transition state) are affected by these patterns, making intuitive predictions concerning the effect of rotation–vibration coupling on microcanonical rate coefficients difficult. Although statistical theories of unimolecular reactions can in principle account for this phenomenon, most implementations do not; quantum implementations are intractable whereas classical ones are inconvenient and numerically intensive. The density of states N appearing in the denominator of the microcanonical rate expression is almost always obtained by separating reactant vibration from rotation and using the equilibrium geometry to assign an overall (rigid) rotational energy. When the reactant molecule contains enough energy to dissociate this is certainly bound to provide a poor description. Strong evidence for this claim has been found in a comparison of statistical model lifetimes to trajectory results for the dissociation of a long-lived collision complex (Wardlaw 1982). The sum of states G appearing in the numerator of the microcanonical rate expression also usually relies, explicitly or implicitly, on a rigid body approximation for rotational energies. For example, in SACM the adiabatic channel curves are interpolations between rigid rotor-harmonic oscillator (RRHO) levels of reactants and products; in FTST the vibrational angular momentum of the conserved modes in the separating fragments is ignored despite the exact (classical) treatment of the transitional modes and adherance to angular momentum coupling restrictions. Troe (1983) has derived various approximate multiplicative factors designed to correct for effects which are neglected in standard RRHO treatments of sums and densities of state. These depend on (E, J) and include an anharmonicity correction and an angular momentum coupling factor to account for the violation of angular momentum coupling restrictions in separable treatments. As noted by Troe, such simplified correction schemes are arbitrary in certain respects and may be of insufficient accuracy when high precision is required.

We conclude with two numerical examples which explore the significance of rotation–vibration coupling for unimolecular rate theory. The first is a comparison of the exact classical sum of states for a rotating Morse oscillator to that resulting from a separation of vibration and rotation (Song and Chesnavich 1989). The ratios of the approximate to exact sum of states for models of three diatomics are plotted as a function of a reduced energy in figure 13. The separable sum of states is seen to become increasingly smaller than the exact result with increasing energy. The ratio is 0·8–0·9 when the energy is half the diatomic dissociation energy. Under thermal conditions the reliability of the separable treatment will depend on temperature which provides a convenient estimate of the *average* energy of a particular mode or fragment.

In the second example we examine the coupling between rotation and transitional/conserved modes in methane decomposition: $CH_4 \rightarrow CH_3 + H$. Coupling coefficients between the reaction coordinate and the various modes orthogonal to the reaction path and between pairs of these modes were obtained as a function of the reaction coordinate and the various modes orthogonal to the reaction path and between pairs of these modes were obtained as a function of the reaction coordinate in the transition state region (Wardlaw 1990) using a $J=0$ reaction path Hamiltonian (Miller *et al.* 1980) on the so-called Hirst potential energy surface (Hase *et al.* 1987). Since C_{3v} symmetry is preserved along the reaction path, states corresponding to different irreducible representations do not interact and have coupling coefficients which are identically zero (Miller 1983). Since the rotation about the symmetry axis is the only degree of freedom corresponding to the A_2 irreducible representation, it does not couple to any other degree of freedom. The doubly degenerate rotation about axes

perpendicular to the symmetry axis (irreducible representation E) can couple to the following (double degenerate) modes of the $H\cdots CH_3$ complex: CH_3 stretch, CH_3 'in-plane' bend, and the transitional mode which is a CH_3 rock in the reactant and a free rotation of the CH_3 product. Nine of fifteen non-zero coupling coefficients are plotted in figure 14 as a function of the C–H separation R which, for this system, is found to be linearly related to the reaction coordinate. In the transition state region (indicated by dashed vertical lines) the rotation–transitional mode coupling coefficient is seen to be comparatively large, as could have been anticipated. The rotation–bend and rotation–stretch coupling coefficients are consistently smaller than the rotation–transitional mode coupling coefficient by approximately a factor of three between the dashed lines. It is worth noting that the reaction path Hamiltonian describes the system only in vicinity of the minimum energy path, thereby modelling the transitional modes as a doubly degenerate vibration. Although the transitional modes are in fact a 2-d hindered rotor whose barrier depends on R, one nevertheless expects relatively strong coupling between this motion and external rotation. A proper description of the transitional modes for this system must account for this coupling as well as the hindered nature of the motion. Flexible transition state theory, which has been applied to $CH_3+H\rightarrow CH_4$ (Aubanel and Wardlaw 1989), is an example of an implementation of RRKM theory which accommodates both features.

Acknowledgments

This research was supported by the National Science Foundation of the United States and the Natural Sciences and Engineering Research Council (NSERC) of Canada. D.M.W. is a University Research Fellow of NSERC.

References

AUBANEL, E. E., and WARDLAW, D. M., 1989, *J. phys. Chem*, **93,** 3117.
AUBANEL, E. E., and WARDLAW, D. M., 1990, *Chem. phys. Lett.*, **167,** 145.
BEYER, T., and SWINEHART, D. F., 1973, *Commun. Assoc. Comput. Mach.*, **16,** 372
BOWMAN, J. M., GAZDY, B., and SUN, Q., 1989, *J. chem. Phys.*, **91,** 2859.
BROUWER, L., COVOS, C. J., TROE, J., DUBAL, H.-R., and CRIM, F. F., 1987, *J. chem. Phys.*, **86,** 6171.
BRUEHL, M., and SCHATZ, G. C., 1988, *J. phys. Chem.*, **92,** 7223.
BUNKER, D. L., and PATTENGILL, M., 1968, *J. chem. Phys.*, **48,** 772.
BUNKER, D. L., 1972, *J. chem. Phys.*, **57,** 332.
CHESNAVICH, W. J., and BOWERS, M. T., 1977a, *J. Am. Chem. Soc.*, **99,** 1705.
CHESNAVICH, W. J., and BOWERS, M. T., 1977b, *J. chem. Phys.*, **66,** 2306.
CHESNAVICH, W. J., and BOWERS, M. T., 1979, *Gas Phase Ion Chemistry*, Vol. 1, edited by M. T. Bowers (Academic Press), p. 119.
COBOS, C. J., and TROE, J., 1985, *J. chem. Phys.*, **83,** 1010.
CRIM, F. F., 1984, *Ann. Rev. phys. Chem.*, **35,** 659.
CURRENT, J. H., and RABINOVITCH, B. S., 1963, *J. chem. Phys.*, **38,** 783.
ELIASON, M. A., and HIRSCHFELDER, J. O., 1959, *J. chem. Phys.*, **30,** 1426.
EZRA, G. S., 1986, *Chem. phys. Lett.*, **127,** 492.
FARLEY, F. W., NOVAKOSKI, L. V., DUBEY, M. K., NATHANSON, G. M., and MCCLELLAND, G. M., 1988, *J. chem. Phys.*, **88,** 1460.
FORST, W., 1973, *Theory of Unimolecular Reactions* (Academic Press).
GILBERT, R. G., LUTHER, K., and TROE, J., 1983, *Ber. Bunsenges. phys. Chem.*, **87,** 169.
GORDON, M. S., and TRUONG, T. N., 1987, *Chem. phys. Lett.*, **142,** 110.
GREEN, W. H., CHEN, I.-C., and MOORE, C. B., 1988, *Ber. Bunsenges. phys. Chem.*, **92,** 389.
HAMILTON, I. P., and BRUMER, P., 1985, *J. chem. Phys.*, **82,** 595.
HASE, W. L., 1976, *J. chem. Phys.*, **64,** 2442.

HASE, W. L., 1976, *Dynamics of Molecular Collisions*, Part B, edited by W. H. Miller (Plenum Press), p. 121.
HASE, W. L., and WOLF, R. J., 1981, *J. chem. Phys.*, **75,** 3809.
HASE, W. L., and SCHLEGEL, H. B., 1982, *J. phys. Chem.*, **86,** 3901.
HASE, W. L., 1983, *Acc. Chem. Res.*, **16,** 258.
HASE, W. L., BUCKOWSKI, D. G., and SWAMY, K. N., 1983, *J. phys. Chem.*, **87,** 2754.
HASE, W. L., MONDRO, S. L., DUCHOVIC, R. J., and HIRST, D. M., 1987, *J. Am. Chem. Soc.*, **109,** 2916.
HASE, W. L., and HU, X., 1989, *J. phys. Chem.*, **93,** 6029.
HASE, W. L., and WARDLAW, D. M., 1989, *Bimolecular Collisions*, edited by M. N. R. Ashfold and J. E. Baggott (Royal Society of Chemistry), p. 171.
HIPPLER, H., TROE, J., and WENDELKEN, H. J., 1983, *J. chem. Phys.*, **78,** 6709 and 6718.
HIRSCHFELDER, J. O., and WIGNER, E., 1939, *J. chem. Phys.*, **7,** 616.
HOFACKER, L., 1963, *Z. Naturf.*, **18A,** 607.
HOLMLID, L., and RYNEFORS, K., 1977, *Chem. Phys.*, **19,** 261.
HU, X., and HASE, W. L., 1989, *Chem. phys. Lett.*, **156,** 115.
KITTRELL, C., ABRAMSON, E., KINSEY, J. L., MCDONALD, S. A., REISNER, D. E., FIELD, R. W., and KATAYAMA, D. H., 1981, *J. chem. Phys.*, **75,** 2056.
KLIPPENSTEIN, S. J., KHUNDKAR, L. R., ZEWAIL, A. H., and MARCUS, R. A., 1988,
KLIPPENSTEIN, S. J., and MARCUS, R. A., 1987, *J. chem. Phys.*, **87,** 3410.
KLIPPENSTEIN, S. J., and MARCUS, R. A., 1988, *J. chem. Phys.*, **92,** 3105.
KLIPPENSTEIN, S. J., and MARCUS, R. A., 1989, *J. chem. Phys.*, **91,** 2280.
KLOTS, C. E., 1971, *J. phys. Chem.*, **75,** 1526.
KLOTS, C. E., 1972, *Z. Naturf.* A, **27,** 553.
KLOTS, C. E., 1976. *J. phys. Chem.*, **64,** 4269.
MARCUS, R. A., and RICE, O. K., 1951, *J. phys. Colloid Chem.*, **55,** 894.
MARCUS, R. A., 1952, *J. chem. Phys.*, **20,** 359.
MARCUS, R. A., 1965, *J. chem. Phys.*, **43,** 2658.
MARCUS, R. A., 1966, *J. chem. Phys.*, **45,** 4493.
MARCUS, R. A., 1975, *J. chem. Phys.*, **62,** 1372.
MARCUS, R. A., 1988, *Chem. phys. Lett.*, **144,** 208.
MILLER, W. B., SAFRON, S. A., and HERSCHBACH, D. R., 1967, *Discuss. Faraday Soc.*, **44,** 108.
MILLER, W. H., 1979, *J. Am. Chem Soc.*, **101,** 6810.
MILLER, W. H., HANDY, N. C., and ADAMS, J. E., 1980, *J. chem. Phys.*, **72,** 99.
MILLER, W. H., 1983, *J. Am. Chem. Soc.*, **105,** 216.
MILLER, W. H., HASE, W. L., and DARLING, C. L., 1989, *J. chem. Phys.*, **91,** 2863.
MONDRO, S. L., VANDE LINDE, S. R., and HASE, W. L., 1986, *J. chem. Phys.*, **84,** 378.
NADLER, I., NOBLE, M., REISLER, H., and WITTIG, C., 1985, *J. chem. Phys.*, **82,** 2608.
NOBLE, M., NADLER, I., REISLER, H., and WITTIG, C., 1984, *J. chem. Phys.*, **81,** 4333.
PARSON, J. M., SHOBATAKE, K., LEE, Y. T., and RICE, S. A., 1973, *Discuss. Faraday Soc.*, **55,** 344.
PECHUKAS, P., and LIGHT, J. C., 1965, *J. chem. Phys.*, **42,** 3281.
PECHUKAS, P., LIGHT, J. C., and RANKIN, C., 1966, *J. chem. Phys.*, **44,** 794.
PITZER, K. S., and GWINN, W. D., 1942, *J. chem. Phys.*, **10,** 428.
QIAN, C. X. W., NADLER, I., NOBLE, M. REISLER, H., and WITTIG, C., 1985, *J. chem. Phys.*, **83,** 5573.
QUACK, M., and TROE, J., 1974, *Ber. Bunsenges. phys. Chem.*, **78,** 240.
QUACK, M., and TROE, J., 1975, *Ber. Bunsenges. phys. Chem.*, **79,** 469.
QUACK, M., and TROE, J., 1977, *Ber. Bunsenges. phys. Chem.*, **81,** 329.
QUACK, M., and TROE, J., 1981, *Theoretical Chemistry: Advances and Perspectives*, Volume 6B, edited by D. Henderson (Academic Press), p. 199.
REDDY, K. W., and BERRY, M. J., 1977, *Chem. phys. Lett.*, **52,** 111.
RICE, O. K., and GERSHINOWITZ, H., 1934,
RIZZO, T. R., HAYDEN, C. C., and CRIM, F. F., 1984, *J. chem. Phys.*, **81,** 450.
RIZZO, T. R., 1990, private communication.
ROBINSON, P. J., and HOLBROOK, K. A., 1972, *Unimolecular Reactions* (Wiley-Interscience).
RYNEFORS, K., 1982, *J. chem. Phys.*, **77,** 6051.
SAFRON, S. A., WEINSTEIN, N. D., HERSCHBACH, D. R., and TULLY, J. C., 1972, *Chem. phys. Lett.*, **12,** 564.
SAHM, D. K., and UZER, T., 1989, *J. chem. Phys.*, **90,** 3159.

SCHNEIDER, F. W., and RABINOVITCH, B. S., 1963, *J. Am. Chem. Soc.*, **84,** 4215.
SHIRTS, R. B., 1987, *Int. J. Quant. Chem.*, **31,** 119.
SMITH, S. C., and GILBERT, R. G., 1988, *Int. J. Chem. Kinetics*, **20,** 307 and 979.
SONG, K., and CHESNAVICH, W. J., 1989, *J. chem. Phys.*, **91,** 4664.
SONG, K., and CHESNAVICH, W. J., 1990, *J. chem. Phys.*, **93,** 5751.
STEIN, S. E., and RABINOVITCH, B. S., 1973, *J. chem. Phys.*, **58,** 2438.
STEINFELD, J. I., FRANCISCO, J. S., and HASE, W. L., 1989, *Chemical Kinetics and Dynamics* (Prentice Hall).
TICIH, T. M., RIZZO, T. R., DUBAL, H.-R., and CRIM, F. F., 1986, *J. chem. Phys.*, **84,** 1508.
TOWNES, C. H., and SCHALOW, A. L., 1955, *Microwave Spectroscopy* (McGraw-Hill), pp. 84–86.
TROE, J., 1977, *J. chem. Phys.*, **66,** 4645.
TROE, J., 1979, *J. Phys. Chem.*, **83,** 114.
TROE, J., 1981, *J. chem. Phys.*, **75,** 226.
TROE, J., 1983, *J. chem. Phys.*, **79,** 6017.
TROE, J., 1987, *J. chem. Phys.*, **87,** 2773.
UZER, T., NATANSON, G. A., and HYNES, J. T., 1985, *Chem. phys. Lett.*, **122,** 12.
VANDE LINDE, S. R., MONDRO, S. L., and HASE, W. L., 1987, *J. chem. Phys.*, **86,** 1348.
VANDE LINDE, S. R., and HASE, W. L., 1990, *J. chem. Phys.*, **93,** 7962.
WAAGE, E. V., and RABINOVITCH, B. S., 1970, *Chem. Rev.*, **70,** 377.
WAGNER, A. F., and WARDLAW, D. M., 1988, *J. phys. Chem.*, **92,** 2462.
WARDLAW, D. M., 1982, Ph.D. Dissertation, University of Toronto.
WARDLAW, D. M., and MARCUS, R. A., 1984, *Chem. phys. Lett.*, **110,** 230.
WARDLAW, D. M., and MARCUS, R. A., 1985, *J. chem. Phys.*, **83,** 3462.
WARDLAW, D. M., and MARCUS, R. A., 1986, *J. phys. Chem.*, **90,** 5383.
WARDLAW, D. M., and MARCUS, R. A., 1988, *Adv. chem. Phys.*, **70,** 231, part I.
WARDLAW, D. M., 1990, unpublished.
WIEDER, G. M., and MARCUS, R. A., 1962, *J. chem. Phys.*, **37,** 1835.
WITIG, C., NADLER, I., REISLER, H., NOBLE, M., CANTANZARITE, J., and RADHAKRISHNAN, G., 1985, *J. chem. Phys.*, **83,** 5581.
WORRY, G., and MARCUS, R. A., 1977, *J. chem. Phys.*, **67,** 1636.
ZHU, L., and HASE, W. L., 1990, *Chem. phys. Lett.*, **175,** 117.
ZHU, L., HASE, W. L., AUBANEL, E. E., and WARDLAW, D. M., 1990, in preparation.